

Washington University School of Medicine

Digital Commons@Becker

2020-Current year OA Pubs

Open Access Publications

1-1-2024

Bioactive glycans in a microbiome-directed food for children with malnutrition

Matthew C Hibberd

Washington University School of Medicine in St. Louis

Daniel M Webber

Washington University School of Medicine in St. Louis

Suzanne Henrissat

Washington University School of Medicine in St. Louis

Robert Y Chen

Washington University School of Medicine in St. Louis

Cyrus Zhou

Washington University School of Medicine in St. Louis

See next page for additional authors

Follow this and additional works at: https://digitalcommons.wustl.edu/oa_4



Part of the [Medicine and Health Sciences Commons](#)

Please let us know how this document benefits you.

Recommended Citation

Hibberd, Matthew C; Webber, Daniel M; Henrissat, Suzanne; Chen, Robert Y; Zhou, Cyrus; Lynn, Hannah M; Wang, Yi; Chang, Hao-Wei; Lee, Evan M; Lelwala-Guruge, Janaki; Chen, Ye; Mostafa, Ishita; Das, Subhasish; Mahfuz, Mustafa; Barratt, Michael J; Ahmed, Tahmeed; Gordon, Jeffrey I; and et al., "Bioactive glycans in a microbiome-directed food for children with malnutrition." *Nature*. 625, 7993. 157 - 165. (2024).
https://digitalcommons.wustl.edu/oa_4/3347

This Open Access Publication is brought to you for free and open access by the Open Access Publications at Digital Commons@Becker. It has been accepted for inclusion in 2020-Current year OA Pubs by an authorized administrator of Digital Commons@Becker. For more information, please contact vanam@wustl.edu.

Authors

Matthew C Hibberd, Daniel M Webber, Suzanne Henrissat, Robert Y Chen, Cyrus Zhou, Hannah M Lynn, Yi Wang, Hao-Wei Chang, Evan M Lee, Janaki Lelwala-Guruge, Ye Chen, Ishita Mostafa, Subhasish Das, Mustafa Mahfuz, Michael J Barratt, Tahmeed Ahmed, Jeffrey I Gordon, and et al.

Bioactive glycans in a microbiome-directed food for children with malnutrition


<https://doi.org/10.1038/s41586-023-06838-3>

Received: 18 March 2022

Accepted: 6 November 2023

Published online: 13 December 2023

Open access

 Check for updates

Matthew C. Hibberd^{1,2,3,11}, Daniel M. Webber^{1,2,3,11}, Dmitry A. Rodionov⁴, Suzanne Henrissat^{1,2,5}, Robert Y. Chen^{1,2}, Cyrus Zhou^{1,2}, Hannah M. Lynn^{1,2}, Yi Wang^{1,2}, Hao-Wei Chang^{1,2}, Evan M. Lee^{1,2}, Janaki Lelwala-Guruge^{1,2}, Marat D. Kazanov⁶, Aleksandr A. Arzamasov⁴, Semen A. Leyn⁴, Vincent Lombard⁵, Nicolas Terrapon⁵, Bernard Henrissat^{7,8}, Juan J. Castillo⁹, Garret Couture⁹, Nikita P. Bacalzo Jr⁹, Ye Chen^{1,2,9}, Carlito B. Lebrilla⁹, Ishita Mostafa¹⁰, Subhasish Das¹⁰, Mustafa Mahfuz¹⁰, Michael J. Barratt^{1,2,3}, Andrei L. Osterman⁴, Tahmeed Ahmed¹⁰ & Jeffrey I. Gordon^{1,2,3,11}✉

Evidence is accumulating that perturbed postnatal development of the gut microbiome contributes to childhood malnutrition^{1–4}. Here we analyse biospecimens from a randomized, controlled trial of a microbiome-directed complementary food (MDCF-2) that produced superior rates of weight gain compared with a calorically more dense conventional ready-to-use supplementary food in 12–18-month-old Bangladeshi children with moderate acute malnutrition⁴. We reconstructed 1,000 bacterial genomes (metagenome-assembled genomes (MAGs)) from the faecal microbiomes of trial participants, identified 75 MAGs of which the abundances were positively associated with ponderal growth (change in weight-for-length *Z* score (WLZ)), characterized changes in MAG gene expression as a function of treatment type and WLZ response, and quantified carbohydrate structures in MDCF-2 and faeces. The results reveal that two *Prevotella copri* MAGs that are positively associated with WLZ are the principal contributors to MDCF-2-induced expression of metabolic pathways involved in utilizing the component glycans of MDCF-2. The predicted specificities of carbohydrate-active enzymes expressed by their polysaccharide-utilization loci are correlated with (1) the in vitro growth of Bangladeshi *P. copri* strains, possessing varying degrees of polysaccharide-utilization loci and genomic conservation with these MAGs, in defined medium containing different purified glycans representative of those in MDCF-2, and (2) the levels of faecal carbohydrate structures in the trial participants. These associations suggest that identifying bioactive glycan structures in MDCFs metabolized by growth-associated bacterial taxa will help to guide recommendations about their use in children with acute malnutrition and enable the development of additional formulations.

The global health challenge of childhood undernutrition is considerable; in 2020, an estimated 149 million children under the age of 5 years had stunted growth (low height for age) while 45 million exhibited wasting (low WLZ)⁵. Undernutrition and its long-term sequelae are the leading causes of morbidity and mortality in individuals of this age range. Sequelae include persistent impairments in linear growth, immune and metabolic functions, and neurodevelopment—all of which have proven to be largely resistant to current interventions⁶. Although food insecurity is not the sole driver of undernutrition⁷, the profound disruption of economies and food systems by the COVID-19 pandemic has greatly exacerbated this global health challenge⁸.

Studies of healthy members of birth cohorts living in several countries have identified shared features of gut microbial community assembly—a process that is largely completed by the end of the second postnatal year^{9,10}. Children with moderate (MAM) or severe (SAM) acute malnutrition have impaired ponderal growth (wasting). Their microbial community development is perturbed, resulting in microbiota configurations that resemble those of chronologically younger children⁹. The metabolic maturation of children with malnutrition is also compromised compared with their healthy peers¹¹. Colonization of gnotobiotic mice with faecal microbiota samples collected from healthy children or from chronologically age-matched children with

¹Edison Family Center for Genome Sciences and Systems Biology, Washington University School of Medicine, St Louis, MO, USA. ²Center for Gut Microbiome and Nutrition Research, Washington University School of Medicine, St Louis, MO, USA. ³Department of Pathology and Immunology, Washington University School of Medicine, St Louis, MO, USA. ⁴Infectious and Inflammatory Disease Center, Sanford Burnham Prebys Medical Discovery Institute, La Jolla, CA, USA. ⁵Architecture et Fonction des Macromolécules Biologiques, CNRS, Aix-Marseille University, Marseille, France. ⁶Faculty of Engineering and Natural Sciences, Sabanci University, Istanbul, Turkey. ⁷Department of Biotechnology and Biomedicine (DTU Bioengineering), Technical University of Denmark, Lyngby, Denmark. ⁸Department of Biological Sciences, King Abdulaziz University, Jeddah, Saudi Arabia. ⁹Department of Chemistry, University of California, Davis, Davis, CA, USA. ¹⁰International Centre for Diarrhoeal Disease Research, Bangladesh (icddr,b), Dhaka, Bangladesh. ¹¹These authors contributed equally: Matthew C. Hibberd, Daniel M. Webber. ✉e-mail: jgordon@wustl.edu

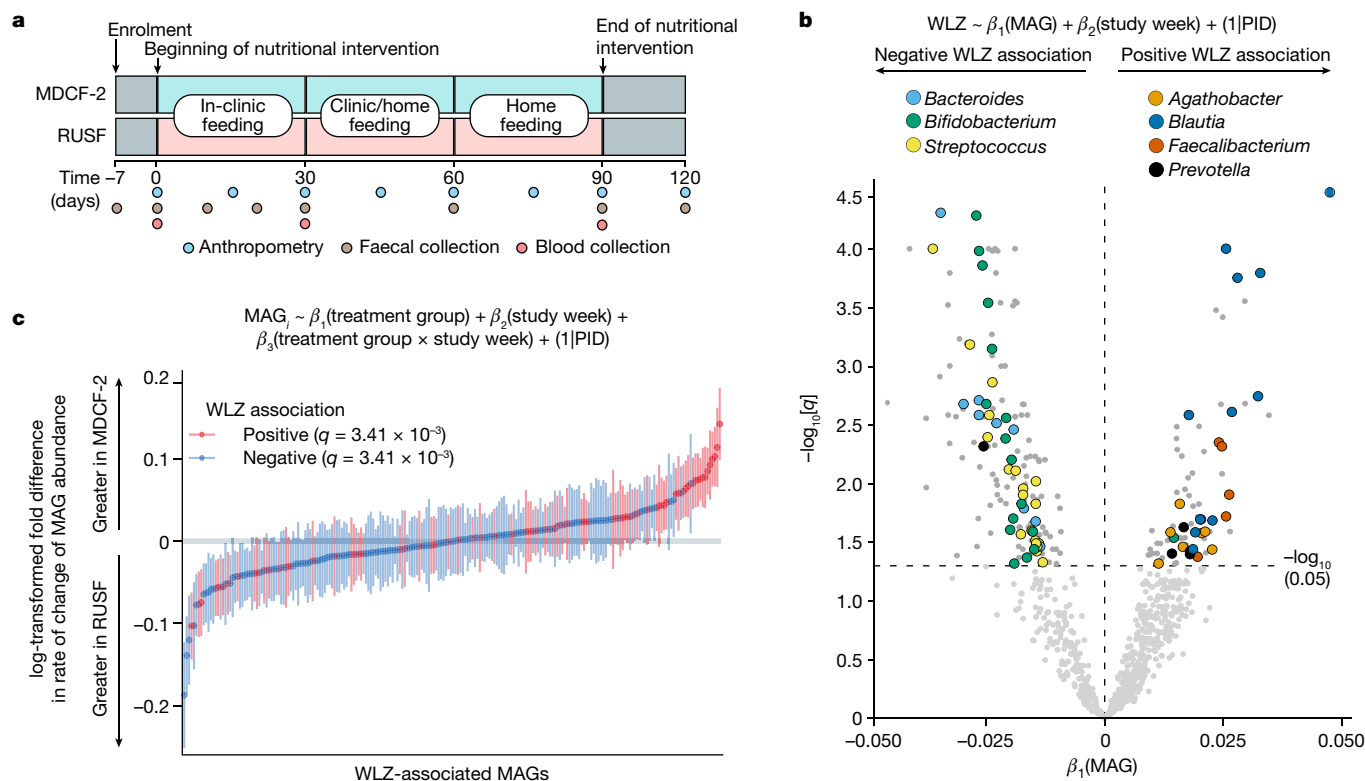


Fig. 1 | Identification of WLZ-associated MAGs. **a**, The human study design. **b**, The results of linear mixed-effects modelling of the relationship (indicated by a -) between MAG abundance and WLZ scores for all of the trial participants, irrespective of treatment. Bacterial genera that are prevalent in the list of MAGs significantly associated with WLZ are coloured by their taxonomic classification. PID, participant identifier. **c**, The results of GSEA of WLZ-associated MAGs ranked according to the magnitude of the difference in their rate of change in

abundance over time in response to MDCF-2 versus RUSF treatment. The plotted values indicate the mean \pm s.e.m. \log_2 -transformed fold change in the $\beta_3(\text{treatment group} \times \text{study week})$ coefficient for 589 biologically independent samples across the $n = 59$ participants assigned to each of the two treatment groups. The statistical significance of enrichment (q value, GSEA) of MAGs that are positively or negatively associated with WLZ is shown.

acute malnutrition revealed that microbial communities from the latter transmitted impaired weight-gain and altered bone-growth phenotypes, and produced immune and metabolic abnormalities^{1,2,12}.

We used gnotobiotic mouse and piglet models to design MDCF formulations for repairing the microbial communities of children with MAM. MAM is defined as having a WLZ score that is 2–3 s.d. below the median of a multinational cohort of age-matched healthy children. In a 3-month randomized controlled feeding study of 12–18-month-old Bangladeshi children with MAM, we demonstrated that a lead formulation (MDCF-2) produced a significant improvement in the rate of weight gain (β -WLZ) compared with a conventional ready-to-use supplementary food (RUSF) that was not designed to alter the gut microbiota⁴. The superior effect of MDCF-2 on β -WLZ occurred even though its caloric density is 15% lower than RUSF. Plasma proteomic analyses revealed 70 proteins of which the levels had statistically significant positive correlations with the change in WLZ, including mediators of musculoskeletal growth and neurodevelopment. These proteins were increased to a significantly greater degree in MDCF-2-treated children compared with in those receiving RUSF. The levels of several proteins involved in immunoinflammatory processes were negatively correlated with WLZ and significantly reduced by MDCF-2 treatment⁴. Sequencing PCR amplicons generated from bacterial 16S rRNA genes present in faecal biospecimens revealed 23 bacterial taxa that were significantly associated with WLZ; 21 were positively associated, whereas two were negatively associated. The abundances of the positively associated taxa increased to a significantly greater degree after treatment with MDCF-2 compared with RUSF⁴.

Here we reconstruct the genomes of bacteria present in the gut communities of the participants in the completed trial, identify metabolic

pathways that are differentially expressed in response to MDCF-2 in MAGs that are positively associated with WLZ and determine how their differential expression relates to the processing of components of MDCF-2 and ponderal growth responses. The results highlight the marked strain specificity of microbiome responses and point to two *P. copri* strains as key mediators of MDCF-2 glycan metabolism and host ponderal growth responses.

Bacteria associated with growth

A summary of the design of the randomized, controlled feeding study of children with MAM, aged 15.4 ± 2.0 months (mean \pm s.d.) at enrolment is shown in Fig. 1a. These children lived in an urban area with high levels of poverty (Mirpur) located in Dhaka, Bangladesh. The 3-month intervention involved twice-daily dietary supplementation with either MDCF-2 or RUSF (two 25 g servings, providing around 220–250 kcal per day)⁴. A total of 59 children in each treatment group completed the intervention and a 1-month follow-up; faecal samples were collected every 10 days during the first month and every 4 weeks thereafter. There were no statistically significant differences in the amount of nutritional supplement consumed between children receiving MDCF-2 versus RUSF, no differences in the proportion of children who satisfied World Health Organization requirements for minimum meal frequency or minimum acceptable diet, and no differences in the amount of breast milk consumed between the two treatment groups⁴.

To reconstruct the genomes of bacterial taxa present in the gut microbiomes of the study participants, we isolated DNA from all of the faecal samples ($n = 942$; 7–8 samples per participant) and performed short-read shotgun sequencing. DNA recovered from faecal

biospecimens collected at $t = 0$ and 3 months from the subset of participants comprising the upper quartile of the ponderal growth response to MDCF-2 ($n = 15$)⁴ were analysed using additional long-read sequencing. We assembled pooled shotgun sequencing data from each participant's faecal samples (short-read only, or short plus long reads when available) and aggregated contigs into MAGs (Extended Data Fig. 1, Methods and Supplementary Discussion). The resulting set of 1,000 high-quality MAGs (defined as $\geq 90\%$ complete and $\leq 5\%$ contaminated based on marker gene analysis; Supplementary Table 1a) represented $65.6 \pm 8.0\%$ and $66.2 \pm 7.9\%$ of all quality-controlled, paired-end shotgun reads generated from all 942 faecal DNA samples analysed in the MDCF-2 and RUSF treatment groups, respectively ($2.3 \pm 1.4 \times 10^7$ 150-nucleotide paired-end reads per sample (mean \pm s.d.); Supplementary Table 2a). Taxonomy was assigned to MAGs¹³ (Supplementary Table 1a). Abundances were calculated for each MAG in the 707 faecal samples that spanned the beginning of treatment to the timepoint at 1-month after intervention and for which matching anthropometric measurements from children had been collected. A total of 837 MAGs satisfied our abundance and prevalence thresholds (Methods and Supplementary Table 2b). We then used linear mixed-effects models to identify 222 MAGs of which the abundances were significantly associated with WLZ ($\beta_i(\text{MAG})$, false-discovery-rate-adjusted $P(q) < 0.05$; Fig. 1b) over the 90-day course of the intervention and 30-day follow-up (the 75 positively associated and 147 negatively associated MAGs are shown in Supplementary Table 3). MAGs that were significantly positively associated with WLZ were predominantly members of the genera *Agathobacter*, *Blautia*, *Faecalibacterium* and *Prevotella*, whereas members of *Bacteroides*, *Bifidobacterium* and *Streptococcus* were prevalent among MAGs that were negatively associated with WLZ (Fig. 1b, Extended Data Fig. 2a and Supplementary Table 3).

Changes in MAG abundances were subsequently modelled as a function of treatment group, study week and the interaction between treatment group and study week, controlling for repeated measurements taken from the same individual (Fig. 1c (equation) and Methods). The 'treatment group \times study week' interaction coefficient in the equation describes the difference in the rate of change in abundance of a given MAG (Fig. 1c). Restricting this analysis to the time of initiation of treatment did not reveal any statistically significant differences in MAG abundances between the two groups ($q > 0.05$, one linear model per MAG; Supplementary Table 3b). Expanding the analysis to include all timepoints from initiation to the end of treatment revealed that, although no individual MAG abundances were significantly associated with MDCF-2 or RUSF consumption, MAGs of which the abundances increased faster in the MDCF-2 group compared with in the RUSF group were significantly enriched for those positively associated with WLZ ($q = 3.41 \times 10^{-3}$, gene set enrichment analysis (GSEA); Fig. 1c). By contrast, MAGs with a higher mean abundance as well as those that increased more rapidly in RUSF-treated children were significantly enriched for those negatively associated with WLZ ($q = 1.57 \times 10^{-9}$ and $q = 3.41 \times 10^{-3}$, respectively; GSEA) (Fig. 1c and Supplementary Table 4).

We used a 'subsystems' approach adapted from the SEED genome annotation platform^{14,15} to identify genes that comprise metabolic pathways represented in WLZ-associated MAGs. To do so, genes were aligned to a reference collection of 2,856 human gut bacterial genomes that had been subjected to *in silico* reconstructions of metabolic pathways reflecting major nutrient biosynthetic and degradative capabilities in mcSEED, a microbial community-centred implementation of SEED¹⁶. We used this reference collection and the procedures described in Supplementary Fig. 1 and the Methods to assign putative functions to a subset of 199,334 proteins in the 1,000 MAGs (Supplementary Table 5); these proteins, which represented 1,308 non-redundant functions, formed the basis for predicting which of 106 metabolic pathways were present or absent in each MAG. This effort generated a set of inferred metabolic phenotypes for each MAG (Supplementary Tables 6 and 7). GSEA disclosed multiple metabolic pathways that are

involved in carbohydrate utilization that were significantly enriched in WLZ-associated MAGs ($q < 0.05$) and in MAGs ranked by their changes in abundance in response to MDCF-2 compared with RUSF treatment. Although other non-carbohydrate pathways were also identified using this approach (for example, those involved in aspects of amino acid and bile acid metabolism), pathways involved in carbohydrate utilization predominated ($P = 0.006$, Fisher's test; Extended Data Fig. 2b and Supplementary Table 8).

Glycan composition of MDCF-2 and RUSF

Before analysing the transcriptional responses of MAGs to each nutritional intervention, we characterized the carbohydrates present in MDCF-2 and RUSF, as well as their constituent ingredients (chickpea flour, soybean flour, peanut paste and mashed green banana pulp in the case of MDCF-2; rice, lentil and milk powder in the case of RUSF (Supplementary Table 9a)). Ultrahigh-performance liquid chromatography–triple quadrupole mass spectrometry (UHPLC–QqQ-MS) was used to quantify 14 monosaccharides and 49 unique glycosidic linkages. Polysaccharide content was defined using a procedure in which polysaccharides were chemically cleaved into oligosaccharides, after which the structures of these liberated oligosaccharides were then used to characterize and quantify their 'parent' polysaccharide¹⁷.

The results revealed that L-arabinose, D-xylose, L-fucose, D-mannose and D-galacturonic acid (GalA) are significantly more abundant in MDCF-2 ($P < 0.05$; *t*-test), as are 14 linkages, eight of which contain these monosaccharides (Extended Data Fig. 3 and Supplementary Table 9b,c,e,f). Integrating the quantitative polysaccharide and glycoside linkage data enabled us to conclude that MDCF-2 contains a significantly greater abundance of galactans and mannans compared with RUSF ($P < 0.05$; *t*-test), whereas RUSF contains significantly more starch and cellulose ($P < 0.05$; *t*-test) (Fig. 2a and Supplementary Table 9d,g). Galactans are represented in MDCF-2 as unbranched β -1,4-linked galactan as well as arabinogalactan I (Fig. 2b). Mannans are present as unbranched β -1,4-linked mannan (β -mannan), galactomannan and glucomannan (Fig. 2c). Arabinan is abundant in both formulations, although the representation of arabinose and glycosidic linkages containing arabinose is significantly greater in MDCF-2 than in RUSF (the results of statistical tests are shown in Extended Data Fig. 3 and Supplementary Table 9e,f). Arabinan in MDCF-2 is largely derived from its soybean, banana and chickpea components, whereas, in RUSF, this polysaccharide originates from rice and lentil (Fig. 2a). Arabinans in both formulations share a predominant 1,5-linked-L-arabinofuranose (Araf) backbone. Soybean arabinans are characterized by diverse side chains composed of 1,2- and 1,3-linked-L-Araf connected by 1,2,3-, 1,2,5- and 1,3,5-L-Araf branch points, whereas chickpea, lentil and banana arabinans primarily contain 1,3-linked side chains from 1,3,5-L-Araf branch points¹⁸ (Supplementary Fig. 3).

MDCF-2 effects on MAG gene expression

Microbial RNA-sequencing (RNA-seq) analysis was performed using RNA isolated from faecal samples collected from all of the study participants just before initiation of treatment, and after 1 month and 3 months of treatment ($n = 350$ samples). Transcripts were then quantified by mapping reads from each sample to MAGs. The resulting counts tables were filtered on the basis of the abundance and prevalence of MAGs in the full set of all faecal samples. These filtering steps were designed to exclude MAGs with minimal contributions to the metatranscriptome from subsequent differential expression analysis (exclusion criteria were benchmarked against a simulated metatranscriptomic dataset using the approach described in the Methods).

We used principal component analysis (PCA) to determine baseline differences in overall (DNA-based) MAG abundance profiles, or the abundance of MAG-derived RNAs in the expressed metatranscriptomes,

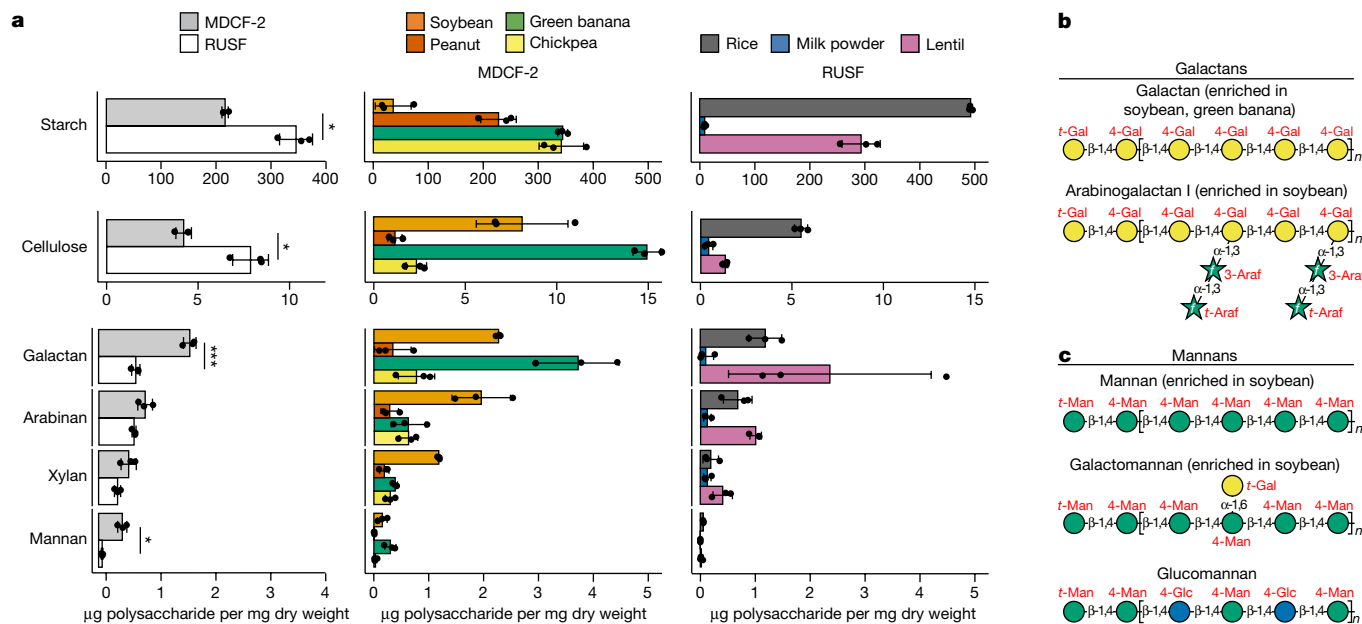


Fig. 2 | Polysaccharides in MDCF-2, RUSF and their component food ingredients. **a**, The principal polysaccharides in MDCF-2, RUSF and their component food ingredients. Data are mean \pm s.d. $n = 3$ measurements of

each food sample. Statistical analysis was performed using two-sided t -tests; $*P < 0.05$, $***P < 0.001$. Points depict technical replicates. **b, c**, The structures of galactans (**b**) and mannans (**c**) in MDCF-2. f, furanose.

between the treatment groups, and to subsequently identify microorganisms that were the principal drivers of shifts during treatment. Figure 3a shows (1) the percentage variance explained by the first principal component (PC) in analyses of 837 MAGs in faecal samples collected across all of the timepoints from all of the study participants and (2) taxa enriched ($q < 0.05$; GSEA) along the first PC of the MAG abundance and metatranscriptome datasets (Fig. 3a; details of analyses of additional PCs are shown in Extended Data Fig. 4). There were no statistically significant differences in the microbiome or metatranscriptome configuration between groups before treatment, or between the MDCF-2 and RUSF groups at each study week ($P > 0.1$; permutational analysis of variance). Analysis of MAG contributions to each PCA highlights the marked enrichment of *Prevotella* spp. transcripts and, to a lesser extent, *Bifidobacterium* spp. transcripts along the principal axis of variation (PC1) of the RNA-based PCA, and, to a much lesser degree, the enrichment of these organisms along PC1 of the DNA-based MAG abundance PCA (Supplementary Table 10).

We subsequently focused on transcripts expressed by the 222 MAGs of which the abundances were significantly associated with WLZ. Transcripts were ranked by their response to MDCF-2 versus RUSF treatment or by their response over time (negative binomial generalized linear model; Fig. 3b (equation)). GSEA was then performed to identify metabolic pathways that were enriched in these ranked transcripts. The analysis revealed an MDCF-2-associated pattern of gene expression characterized by significant enrichment ($q < 0.1$; GSEA) of three metabolic pathways related to carbohydrate utilization (α -arabino oligosaccharide (aAOS), arabinose and fucose; Fig. 3b), three pathways related to de novo amino acid synthesis (arginine, glutamine and lysine) and one pathway for de novo vitamin synthesis (folate; Supplementary Tables 11 and 12). By contrast, none of the 106 metabolic pathways exhibited statistically significant enrichment in their expression in children who received RUSF.

We next investigated which MAGs were responsible for the observed enrichment of expressed pathways. To do so, we turned to 'leading-edge transcripts', a term defined by GSEA as those transcripts that are responsible for enrichment of a given pathway (Methods). Among the positively WLZ-associated MAGs, two MAGs belonging to *P. copri* (MAG Bg0018 and MAG Bg0019) were the source of 11 out of the 14

leading-edge transcripts related to aAOS utilization (Supplementary Table 12)—a pathway of which expression was significantly elevated in children treated with MDCF-2 compared with RUSF (Fig. 3b). Of the 11 *P. copri* MAGs in our dataset, these two were the only MAGs assigned to this species of which the abundances were significantly positively correlated with WLZ. Both MAGs are members of a *P. copri* clade (clade A) that is broadly distributed geographically^{19,20} (Supplementary Fig. 4a; see Supplementary Fig. 4b for the predicted carbohydrate-utilization pathways represented in all 51 MAGs assigned to the genus *Prevotella* that were identified in our 1,000-MAG dataset).

Although *P. copri* MAGs were the greatest source of leading-edge transcripts related to arabinose and aAOS utilization, other MAGs in the microbiome display expression responses consistent with their participation in metabolizing MDCF-2 glycans (or their breakdown products); these include MAGs that are negatively correlated with WLZ. For example, leading-edge transcripts assigned to aAOS, arabinose and fucose utilization also arose from MAGs assigned to *Bifidobacterium longum* ssp. *longum* (Bg0006), *Bifidobacterium longum* ssp. *suis* (Bg0001), *Bifidobacterium breve* (Bg0010; Bg0014), *Bifidobacterium* sp. (Bg0070) and *Ruminococcus gnavus* (Bg0067) (Supplementary Table 12). Features of the metabolism of these glycans in *Bifidobacterium* and *Ruminococcus* MAGs are distinct from those expressed by the *P. copri* MAGs. For example, *B. longum* ssp. *longum* MAG Bg0006 encodes an extracellular exo- α -1,3-arabinofuranosidase that belongs to glycoside hydrolase (GH) family 43_22; this enzyme cleaves terminal 1,3-linked-L-Araf residues present at the ends of branched arabinans and arabinogalactans, two abundant glycans found in MDCF-2^{21,22} (Fig. 2b and Supplementary Fig. 2). By contrast, *P. copri* possesses an endo- α -1,5-L-arabinanase that cleaves interior α -1,5-L-Araf linkages, generating aAOS. Integrating these predictions suggests a complex set of interactions between primary arabinan degraders such as *P. copri* and members of *B. longum*, such as Bg0001 and Bg0006, that have the ability to metabolize products of arabinan degradation (see Supplementary Fig. 5 for reconstructions of carbohydrate-utilization pathways in *Bifidobacterium* MAGs). We cannot discern whether the arabinose available to *Bifidobacterium* is derived from free arabinose or the breakdown products of arabinan polysaccharides. It is important to consider that, in these 12- to 18-month-old children with MAM,

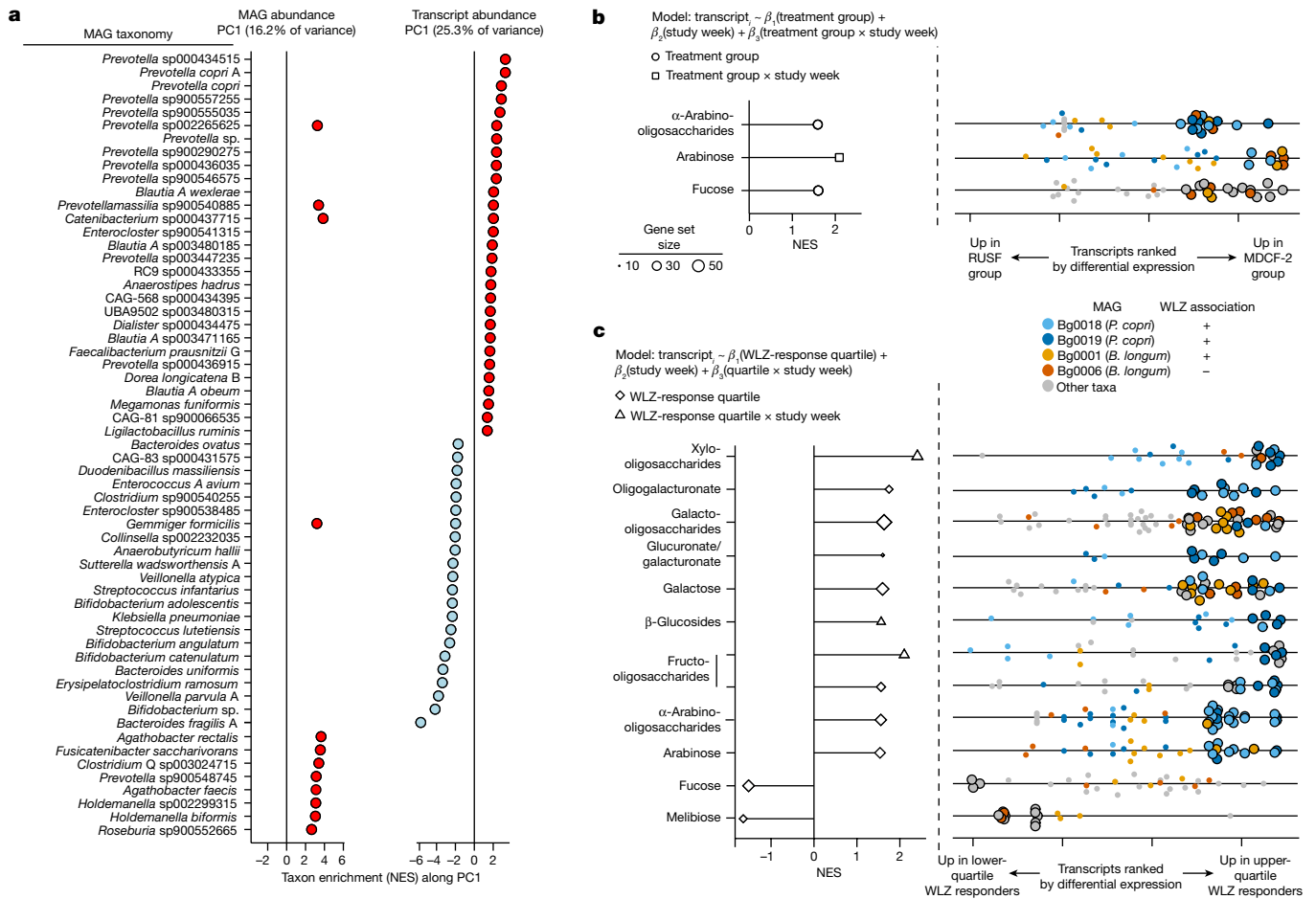


Fig. 3 | Principal taxonomic features and expressed functions of the faecal microbiomes of MDCF-2- and RUSF-treated individuals. a, Significant enrichment of taxa ($q < 0.1$; GSEA) along PC1 of MAG abundance or transcript abundance. NES, normalized enrichment score. **b**, Carbohydrate-utilization pathways significantly enriched ($q < 0.1$; GSEA) by treatment group (β_1 , circles) or the interaction of treatment group and study week (β_3 , squares). Right, each point represents a MAG transcript assigned to each of the indicated functional pathways (rows), ranked according to the direction and statistical significance of their differential expression in MDCF-2 versus RUSF treated participants (defined as the direction of the fold change $\times -\log_{10}[P]$). Transcripts are coloured by their MAGs of origin. The larger, black outlined circles indicate leading-edge

responses to MDCF-2 are occurring in the context of the underlying co-development of their microbial community and host biology, during the period of transition from exclusive milk feeding to a fully weaned state. A MAG defined as positively associated with WLZ by linear modelling is an organism of which the fitness (abundance) increases as WLZ increases. Our studies in healthy 1- to 24-month-old children living in Mirpur have documented how *B. longum* and other members of *Bifidobacterium* decrease in absolute abundance during the period of complementary feeding²³. For the negatively WLZ-associated *Bifidobacterium* MAGs described above, the levels of consumption of MDCF-2 metabolic products during the period of complementary feeding may not be sufficient to overcome a more dominant effect exerted on their abundance/fitness by the state of community–host co-development. Moreover, the metabolic capacities of *B. longum* including, as well as beyond, those related to the processing of MDCF-2 glycans, may influence host growth despite *B. longum* being naturally depleted over developmental time.

On the basis of these observations, we sought further evidence that the two *P. copri* MAGs are related to the magnitude of ponderal growth

transcripts assigned to the pathway described on the left. **c**, Carbohydrate-utilization pathways significantly enriched ($q < 0.1$; GSEA) in upper-versus lower-quartile WLZ responders (β_1 , diamonds), or the interaction between WLZ-response quartile and study week (β_3 , triangles) (see linear mixed-effects model in the Methods section ‘Microbial RNA-seq analysis of MAG gene expression’). Right, transcripts assigned to each functional pathway. The colouring and outlining of circles have the same meaning as in **b**. The enrichment of glucuronate and galacturonate pathways was driven by the same transcripts; these pathways were therefore considered to be a single unit. Supporting information is provided in Supplementary Tables 10–14.

responses and to levels of faecal glycan structures generated from MDCF-2 metabolism.

Glycan utilization and clinical responses

PUL conservation in *P. copri* MAGs

As noted above, the primary outcome measure of the clinical trial was the rate of change of WLZ over the 3-month intervention. We stratified participants receiving MDCF-2 into WLZ-response quartiles⁴ and focused our analysis on (1) children in the WLZ-response upper and lower quartiles ($n = 15$ per group) and (2) transcripts expressed by the 222 MAGs of which the abundances were significantly associated with WLZ. We tested for enrichment of carbohydrate-utilization pathways in transcripts rank-ordered by the strength and direction of their relationship with WLZ-response quartile or, in a separate analysis, the interaction between the WLZ-response quartile and the study week. We next performed GSEA to identify enriched pathways (Supplementary Tables 13 and 14). Eight carbohydrate-utilization pathways were significantly enriched in transcripts that were differentially

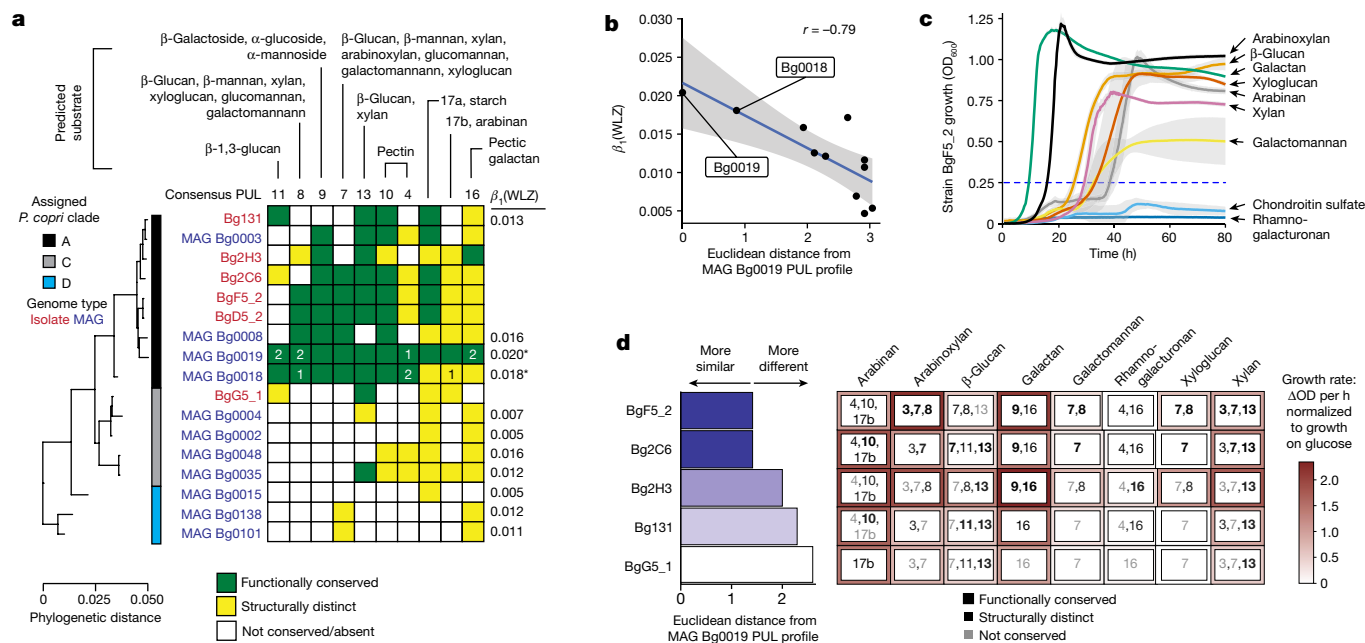


Fig. 4 | Conservation and expression of PULs in *P. copri* MAGs and isolates. **a**, PUL conservation in *P. copri* MAGs identified in study participants (blue font) and in *P. copri* isolates cultured from Bangladeshi children (red font). The marker-gene-based phylogenetic tree (left) indicates the relatedness of *P. copri* MAGs and isolates. The β_1 (WLZ) coefficient for each MAG is shown on the right; significant associations ($q < 0.05$) are indicated by asterisks. The matrix in the centre depicts PUL conservation among *P. copri* MAGs and cultured isolates relative to Bg0019. The number of differentially expressed PUL transcripts in MAGs Bg0018 and Bg0019 are shown within the coloured cells (identified from comparisons of MDCF-2- versus RUSF-treated participants, and/or from MDCF-2-treated participants in the WLZ-response upper versus lower quartiles; transcript annotations are shown in Supplementary Table 15). **b**, The relationship between PUL conservation in the 11 *P. copri* MAGs identified in study participants and the association of each MAG abundance with WLZ. The grey ribbon indicates

the 95% confidence interval. **c, d**, In vitro growth assays for five *P. copri* isolates in defined medium supplemented with individual purified glycans representative of those in MDCF-2. $n = 3$ replicates per condition; two independent experiments were performed; representative results from one are shown. **c**, The results obtained with *P. copri* BgF5_2, the isolate of which the PUL profile is most similar to MAGs Bg0019/Bg0018. Data are the mean \pm s.d. (grey ribbons) optical density at 600 nm (OD₆₀₀). **d**, Summary of PUL conservation and growth rates for the five *P. copri* strains tested (Extended Data Fig. 5a). Each coloured box lists PULs in each strain (rows) that are predicted to metabolize each carbohydrate. PULs are denoted as functionally conserved (black, bold), structurally distinct but functionally similar (black, not bold) or not conserved (grey) according to the scheme shown in **a**. The colour intensity surrounding each box indicates the mean maximum growth rate for each isolate in the presence of each glycan.

expressed in the upper- compared with lower-quartile WLZ responders. One of these pathways (fructooligosaccharide utilization) as well as three other pathways that are involved in arabinose, β -glucoside and xylooligosaccharide utilization were enriched in transcripts with a positive ‘WLZ quartile \times study week’ interaction coefficient (β_3), suggesting that the extent of the difference in expression of these pathways increases over the course of treatment (Fig. 3c and Supplementary Table 14a; see Supplementary Table 14b for enrichment of expressed vitamin and amino acid biosynthetic pathways related to WLZ-response quartile).

Notably, over half of the leading-edge transcripts (67 out of 99; 68%) from the eight, WLZ-response upper-quartile-enriched carbohydrate-utilization pathways were expressed by *P. copri* MAGs Bg0018 and Bg0019. Moreover, these two MAGs contributed no leading-edge transcripts to WLZ-response lower-quartile-enriched pathways.

P. copri is a member of the phylum Bacteroidota. Members of this phylum contain syntenic sets of genes known as polysaccharide-utilization loci (PULs) that mediate the detection, import and metabolism of a specific glycan or set of glycans²⁴. To further define how expressed genomic features distinguish the capacity of MAGs Bg0018 and Bg0019 to respond to MDCF-2, we identified PULs in these MAGs and compared them to PULs present in the nine other *P. copri* MAGs in this study. These two WLZ-associated *P. copri* MAGs share (1) seven PULs that we designated as conserved (that is, pairwise comparisons of open reading frames (ORFs) satisfy the requirements that their protein products have greater than 90% amino acid identity and are organized in an identical way within the respective genomes); and (2) three PULs

designated as present but structurally distinct (that is, a given PUL is present in the genomes being compared but component CAZymes or SusC/SusD proteins are missing or fragmented in a way that is likely to affect their function, or where extra ORFs are present; Methods). The representation of these 10 PULs varied among the other nine *P. copri* MAGs, which span three of the four principal clades of this organism (Fig. 4a and Supplementary Table 15). Notably, the degree of genomic conservation of these PULs is significantly associated with the strength of WLZ association for each of the 11 *P. copri* MAGs in our MAG dataset across both treatment groups (Pearson r between the Euclidean distance from Bg0019 PUL profile and β_1 (MAG) = -0.79 ($P = 0.0035$); Fig. 4b and Supplementary Table 3 (WLZ associations)). Five of the seven highly conserved PULs are related to utilization of mannan and galactan—glycans that are significantly more abundant in MDCF-2 than RUSF. Expression of three of these seven PULs, as well as two of the conserved but structurally distinct PULs, is also related to the enrichment of transcripts in carbohydrate-utilization pathways that distinguish upper- from lower-quartile WLZ responders (‘WLZ-response quartile’ or ‘WLZ quartile \times study week’ terms in Fig. 3c). PULs that generate these leading-edge transcripts are predicted to metabolize β -glucan, glucomannan, β -mannan, xylan, pectin/pectic galactan and arabinogalactan (Fig. 4a shows which of these 10 PULs contribute differentially expressed transcripts; Supplementary Table 15).

A comparative analysis of MAGs Bg0018 and Bg0019 and 22 reference *P. copri* genomes in PULDB²⁵ indicated that one of the highly conserved PULs (PUL7) contains a bimodular GH26|GH5_4 β -glycanase with 52% amino acid sequence identity to an enzyme that is known to cleave

β -glucan, β -mannan, xylan, arabinoxylan, glucomannan and xyloglucan^{26,27} (Fig. 4a and Supplementary Table 15). The gene encoding this multifunctional enzyme did not satisfy our criteria for statistically significant differential expression between MDCF-2 and RUSF treatment, nor between upper- versus lower-quartile WLZ responders. However, it was consistently expressed across these conditions and comparisons (Supplementary Table 15) and its enzymatic product is expected to contribute to the utilization of a broad range of plant glycans, including those represented in MDCF-2.

Together, these results highlight both the versatility in carbohydrate metabolic capabilities of these two WLZ-associated *P. copri* MAGs, as well as the specificity of their treatment-inducible metabolic pathways for carbohydrates prominently represented in MDCF-2.

Effect of carbohydrates on growth of *P. copri* isolates

To contextualize our observations regarding conserved polysaccharide degradation features of *P. copri* MAGs, we engaged in an extensive effort to culture and characterize representatives of these MAGs from faecal samples obtained from the participants in this clinical trial, plus a previous, shorter duration pilot study of MDCF prototypes³. Based on this effort, we selected a set of six *P. copri* isolates that represented diverse repertoires of conserved PULs as well as a range of phylogenetic distances from the WLZ-associated MAGs Bg0018 and Bg0019 (Fig. 4a and Supplementary Table 1b). Strains BgD5_2 and BgF5_2 are highly related phylogenetically to each other and to MAGs Bg0018 and Bg0019. Notably, they possess 9 of the 10 conserved PULs in these MAGs (see Supplementary Tables 7c and 15b for more details of the functional conservation between the genomes of these and the other cultured *P. copri* strains and MAGs). On the basis of the substrate predictions for each conserved PUL, the measured glycan components of MDCF-2, and the variation in conservation of these PULs across our *P. copri* MAGs and isolates, we selected eight candidate glycan substrates for in vitro screening: sugar beet arabinan, wheat arabinoxylan, barley β -glucan, potato galactan, carob galactomannan, soybean rhamnogalacturonan, tamarind xyloglucan and beechwood xylan (Supplementary Table 16a). Chondroitin sulfate was included in the panel as a negative control given its resistance to degradation by *P. copri*²⁸. Each cultured isolate was grown in a defined medium containing 1% (w/v) of each glycan as the sole carbon source, and growth was determined by tracking the OD over time (Fig. 4c and Extended Data Fig. 5a). Strain BgD5_2 displayed poor and inconsistent growth in this medium compared with BgF5_2, even when glucose was used as the sole carbon source; therefore, the BgD5_2 isolate was not included in these in vitro experiments. The results underscore the broad glycan-utilization abilities of the *P. copri* isolates but also highlight their distinct preferences for individual glycans. Figure 4c,d, Extended Data Figs. 5 and 6 and Supplementary Table 16b–d demonstrate that the growth phenotypes of these isolates are aligned with their PUL repertoires; show the known and predicted substrate specificities of the carbohydrate-active enzymes (CAZymes) encoded by their PULs; and present the results of MS-based quantification of their consumption of monosaccharide components of the tested glycans. Isolates of which the PUL profiles matched the two WLZ-associated MAGs most closely (BgF5_2, Bg2C6, Bg2H3) displayed the strongest preference for glycan substrates that were enriched in and/or unique to MDCF-2 relative to RUSF, including arabinans (arabinan, arabinoxylan) and galactans and mannans (galactan, galactomannan) (Fig. 2 and Supplementary Fig. 2). Notably, strain BgF5_2 displayed growth preferences for arabinoxylan and galactan; whereas all of the other strains favoured arabinan over arabinoxylan. Together, these results support predictions of the abilities of the two WLZ-associated MAGs to utilize MDCF-2 glycans; they also indicate that BgF5_2 could be considered to be a cultured representative of Bg0018 and Bg0019 given its similar glycan utilization preferences/capacities to those predicted for these two MAGs.

Faecal glycosidic linkage levels and WLZ responses

The same faecal samples used for the DNA- and RNA-level analyses were processed for UHPLC–QqQ-MS-based quantification of 49 glycosidic linkages. This analysis focused on samples collected at the 0- and 3-month timepoints from MDCF-2-treated individuals in the upper and lower quartile of WLZ response. These linkages were measured after their liberation by in vitro hydrolysis of faecal glycans (Supplementary Table 17). We used linear mixed-effects modelling to compare the changes in levels of faecal glycosidic linkages from the baseline/pre-intervention to the treatment endpoint (3 months) as a function of WLZ-response quartile. The results demonstrated that, with treatment, the levels of 14 linkages increased significantly more ($q < 0.05$) in members of the WLZ-response upper compared with lower quartile. None of the 49 linkages increased significantly more in children who were in the lower compared with upper quartile of WLZ response (Fig. 5a, Extended Data Fig. 7a and Supplementary Table 18a). All 14 glycosidic linkages that were elevated in upper-quartile responders are represented in MDCF-2 (for example, 4,6-mannose, which is predicted to be a product of soybean galactomannan cleavage by endo-1,4- β -mannosidases encoded by PUL7 and PUL8 present in the two WLZ-associated MAGs (Fig. 5b and Supplementary Table 9c); the likely polysaccharide sources of these 14 linkages in MDCF-2 are shown in Fig. 5a).

The levels of glycosidic linkages in the faeces reflect a complex dynamic that includes, but is not necessarily limited to, the substrate specificities of the CAZymes encoded and expressed by PULs in primary consumers of available polysaccharides, the levels of host consumption of MDCF-2 and components of their ‘background’ diets, and the degree to which the initial products of polysaccharide degradation can be further processed by community members. These points are illustrated by the following observations. First, the presence of the 14 glycosidic linkages in the faeces can be explained in part by the specificity of CAZymes encoded and expressed by PULs conserved between *P. copri* MAGs Bg0018 and Bg0019. Figure 5b,c and Extended Data Figs. 7b, 8 and 9 describe which of their PULs are predicted to generate glycan fragments containing these linkages—predictions that are supported by the in vitro data generated from the cultured representative of the two MAGs. For example, *t*-Araf, 5-Araf, 2-Araf and 2,3-Araf are components of polysaccharides (arabinan, arabinoxylan and arabinogalactan type I/II) present in soybean, chickpea, peanut and banana. CAZymes encoded by *P. copri* Bg0019 PULs 4, 7, 8, 16 and 17b have substrate specificities that enable them to cleave accessible linkages in these polysaccharides (Fig. 5b,c and Extended Data Figs. 7b and 9). Some of the products of these cleavage events are probably resistant to further degradation. The exo- α -1,2/1,3-L-arabinofuranosidase and endo- α -1,5-L-arabinanase activities encoded by PUL17b (Fig. 5c) are predicted to remove successive residues from the 1,2- and 1,3-linked-L-Araf chains of branched arabinan and hydrolyse the 1,5-linked-L-Araf backbone from this polysaccharide, yielding an enzyme-resistant product containing *t*-Araf, 5-Araf, 2-Araf and 2,3-Araf linkages. Second, CAZyme transcripts assigned to PULs 4, 7, 8, 16 and 17b were detectable in the faecal metatranscriptomes of all but 1 of the 30 participants assigned to the WLZ-responder upper or lower quartiles. The levels of expression of the majority of these CAZymes genes were modestly elevated in upper-quartile compared with the lower-quartile WLZ responders over the course of treatment, although the difference did not reach our threshold cut-off for statistical significance ($q < 0.05$). These transcripts include the GH51 encoded by PUL17b plus the GH26, GH26/GH5_4, GH130 and carbohydrate esterase family 7 (CE7) transcripts from PUL7 (Extended Data Fig. 7b). Third, while intake of MDCF-2 was not significantly different between the upper- and lower-quartile WLZ participants ($P > 0.05$; linear mixed-effects model), data from a food frequency questionnaire administered at the time of each faecal sampling disclosed a positive correlation between consumption of legumes and nuts and the levels of *t*-Araf, 5-Araf, 2,3-Araf, *t*-GalA and 2,4,6-glucose

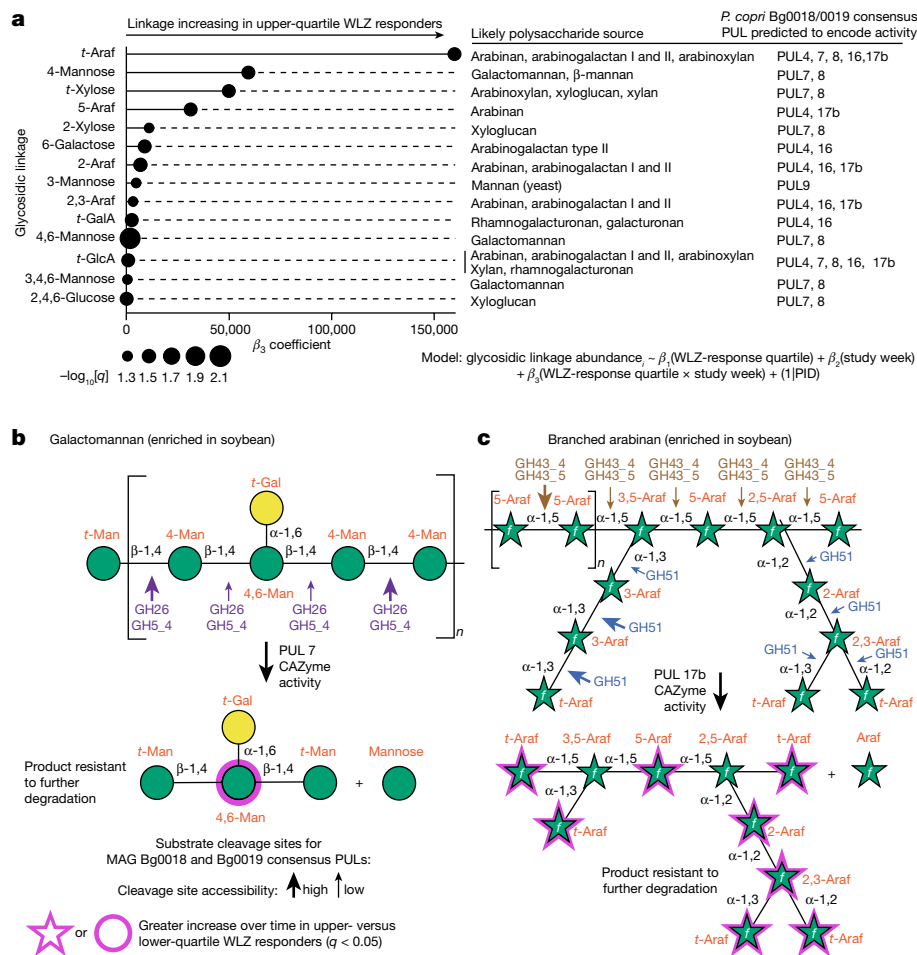


Fig. 5 | Treatment-responsive glycosidic linkages, structures of their polysaccharide sources, cleavage sites and predicted products of CAzyme activity. **a**, Significant changes in faecal glycosidic linkage levels ($q < 0.05$) over time in upper- compared with lower-quartile WLZ responders. Probable polysaccharide sources for each of the 14 glycosidic linkages are noted in the middle (Supplementary Fig. 3). PULs present in *P. copri* MAGs Bg0018 and Bg0019 with known or predicted cleavage activity for the listed polysaccharide sources are noted on the right. **b,c**, The structures of the MDCF-2 polysaccharides

galactomannan (**b**) and branched arabinan (**c**), plus glycan fragments and their constituent glycosidic linkages predicted to be liberated by PULs conserved between *P. copri* MAGs Bg0019 and Bg0018 (the results of PUL conservation analysis are shown in Fig. 4a). The arrows indicate putative sites of cleavage by CAZymes according to their known or predicted enzyme activities. The size of each arrow (large versus small) denotes the relative likelihood (high versus low, respectively) of glycosidic linkage cleavage by the indicated CAZymes, considering steric hindrance at glycan branch points.

(Supplementary Table 18b). Consumption of these foods was also the most discriminatory response between upper-quartile compared with lower-quartile WLZ responders (Supplementary Table 18c). These observations suggest that children consuming more of the classes of complementary food ingredients present in MDCF-2 may also exhibit enhanced growth responses.

The confounding effects of background diet and the role of *P. copri* in processing MDCF-2 glycans can be directly tested in gnotobiotic mice colonized with a defined community of cultured representatives of WLZ-associated MAGs. One such gnotobiotic model is described in our ‘reverse translation’ study in which mice were colonized with a defined consortium of age- and WLZ-associated bacterial strains from Bangladesh, with or without *P. copri* isolates that captured key features of the carbohydrate metabolic apparatus present in Bg0018 and Bg0019 (such as BgF5_2/BgD5_2) and fed either MDCF-2 or a diet representative of that consumed by children living in Mirpur. Analyses revealed that these *P. copri* strains were the principal mediators of MDCF-2 glycan degradation in vivo and that the combination of the presence of *P. copri* and MDCF-2 diet was associated with promoting ponderal growth and had marked effects on multiple aspects of metabolism in intestinal epithelial cell lineages²⁹.

Discussion

Here we illustrate an approach for characterizing the gut microbiome targets and structure–function relationships of a therapeutic food—in this case, MDCF-2. MDCF-2 produced significantly greater weight gain during a 3-month, randomized controlled study of 12- to 18-month-old Bangladeshi children with MAM compared with a conventional, more calorically dense RUSF. We focused on MAGs, specifically (1) treatment-induced changes in the expression of carbohydrate metabolic pathways in MAGs whose abundances were significantly associated with weight gain (WLZ); and (2) MS analysis of the metabolism of glycans present in the two food formulations. Quantifying monosaccharides, glycosidic linkages and polysaccharides present in MDCF-2, RUSF and their component ingredients revealed that MDCF-2 contains more galactans and mannans (for example, galactan, arabinogalactan I, galactomannan, β -mannan and glucomannan). Two types of comparisons were performed of the transcriptional responses of MAGs that were significantly associated with WLZ: one involved study participants who had consumed MDCF-2 versus RUSF, and the other focused on MDCF-2-treated children in the upper versus lower quartiles of WLZ response. The results revealed that two *P. copri* MAGs,

both positively associated with WLZ, were the principal contributors to MDCF-2-induced expression of metabolic pathways involved in the utilization of its component glycans.

Using UHPLC–QqQ-MS, we were able to identify statistically significant changes in glycan composition in the faeces of children consuming a therapeutic food, even in the face of complex and varied background diets. Notably, although the intake of MDCF-2 did not differ between children in the upper and lower quartiles of clinical (WLZ) response, children in the upper quartile trended toward diets containing more legumes and nuts compared with those in the lower quartile. The legumes and nuts food group includes major components of MDCF-2. We postulate that MDCF-2 ‘kick starts’ a microbiome response that includes changes in the fitness and expressed metabolic functions of key growth-associated bacterial strains, such as *P. copri*. Background diet can further modify this response, as evidenced by the higher levels of microbial metabolic products of legume/nut-associated glycans in the faeces of children displaying upper-quartile WLZ responses. This observation also suggests that further optimization of the dose of MDCF-2 may be possible; in our study, MDCF-2 was administered as a dietary supplement designed to provide around 20% of the children’s daily energy requirements. More detailed, quantitative assessments of food consumption during future clinical studies of MDCF-2 could not only facilitate the design of improved formulations/doses but also inform future recommendations regarding complementary feeding practices—recommendations that recognize the important role of the gut microbiome in the healthy growth of children.

One definition of ‘microbiome repair’ in children with malnutrition is a rebalancing of the representation and expressed functions of beneficial organisms so that it assumes a configuration that is more conducive to healthy microbiome–host co-development. Linking dietary glycans and microbial metabolism in this manner provides a starting point for culture-based initiatives designed to retrieve isolates of these ‘effector’ taxa for use as potential probiotic agents, or if combined with key nutrients that they covet, synbiotic formulations for repairing perturbed microbiomes that are insufficiently responsive to food-based interventions alone.

The link between MDCF-2 treatment, *P. copri* glycan metabolism and ponderal growth is not formally established by the data described in this Article. Much remains to be discovered about how MDCF-2 treatment is related to weight gain and healthy growth. For example, further work is needed to clarify whether the mediators of *P. copri* effects on the host arise from direct products of its metabolism of MDCF-2 glycans, or whether products of other metabolic pathways in *P. copri*, of which the activities are regulated by biotransformation of MDCF-2 glycans, are involved. Moreover, the contributions of metabolites from other community members to these effects are unclear. Furthermore, the observed relationships between strains of *P. copri* and MDCF-2 glycans do not exclude the contribution of other macro- or micronutrients to the superiority of MDCF-2 over RUSF on weight gain in our study. Direct tests of the role of organisms such as *P. copri* in mediating microbial community and host responses to components of microbiome-targeted therapeutic foods can come from additional clinical studies of probiotic or synbiotic formulations consisting of strains that are closely related to WLZ-associated MAGs, such as *P. copri* BgF5_2, administered in conjunction with MDCF-2 or with its glycan components. Another approach that we are using involves reverse-translation experiments that use gnotobiotic mice (1) colonized with defined collections of various combinations of cultured, WLZ-associated gut bacterial taxa, with or without *P. copri* strains, and (2) fed diets with or without MDCF-2, or various combinations of its component glycans²⁹.

Online content

Any methods, additional references, Nature Portfolio reporting summaries, source data, extended data, supplementary information,

acknowledgements, peer review information; details of author contributions and competing interests; and statements of data and code availability are available at <https://doi.org/10.1038/s41586-023-06838-3>.

- Smith, M. I. et al. Gut microbiomes of Malawian twin pairs discordant for kwashiorkor. *Science* **339**, 548–554 (2013).
- Blanton, L. V. et al. Gut bacteria that prevent growth impairments transmitted by microbiota from malnourished children. *Science* **351**, aad3311 (2016).
- Gehrig, J. L. et al. Effects of microbiota-directed foods in gnotobiotic animals and undernourished children. *Science* **365**, eaau4732 (2019).
- Chen, R. Y. et al. A microbiota-directed food intervention for undernourished children. *N. Engl. J. Med.* **384**, 1517–1528 (2021).
- Levels and Trends in Child Malnutrition: UNICEF/WHO/The World Bank Group Joint Child Malnutrition Estimates: Key Findings of the 2021 Edition* (WHO, 2021).
- Victoria, C. G. et al. Revisiting maternal and child undernutrition in low-income and middle-income countries: variable progress towards an unfinished agenda. *Lancet* **397**, 1388–1399 (2021).
- Heidkamp, R. A. et al. Mobilising evidence, data, and resources to achieve global maternal and child undernutrition targets and the sustainable development goals: an agenda for action. *Lancet* **397**, 1400–1418 (2021).
- Robertson, T. et al. Early estimated of the indirect effects of COVID-19 pandemic on maternal and child mortality in low-income and middle-income countries; a modelling study. *Lancet Glob. Health* **8**, e901–e908 (2020).
- Subramanian, S. et al. Persistent gut microbiota immaturity in malnourished Bangladeshi children. *Nature* **510**, 417–421 (2014).
- Raman, A. S. et al. A sparse covarying unit that describes healthy and impaired human gut microbiota development. *Science* **365**, eaau4735 (2019).
- Giallourou, N. et al. Metabolic maturation in the first 2 years of life in resource-constrained settings and its association with postnatal growths. *Sci. Adv.* **6**, eaay5969 (2020).
- Kau, A. L. et al. Functional characterization of IgA-targeted bacteria taxa from undernourished Malawian children that produce diet-dependent enteropathy. *Sci. Transl. Med.* **7**, 276ra24 (2015).
- Chaumeil, P. A., Mussig, A. J., Hugenholtz, P. & Parks, D. H. GTDB-Tk: a toolkit to classify genomes with the Genome Taxonomy Database. *Bioinformatics* **36**, 1925–1927 (2020).
- Overbeek, R. et al. The subsystems approach to genome annotation and its use in the project to annotate 1000 genomes. *Nucleic Acids Res.* **33**, 5691–5702 (2005).
- Aziz, R. K. et al. SEED servers: high-performance access to the SEED genomes, annotations, and metabolic models. *PLoS ONE* **7**, e48053 (2012).
- Rodionov, D. A. et al. Micronutrient requirements and sharing capabilities of the human gut microbiome. *Front. Microbiol.* **10**, 1316 (2019).
- Amicucci, M. J. et al. A nonenzymatic method for cleaving polysaccharides to yield oligosaccharides for structural analysis. *Nat. Commun.* **11**, 3963 (2020).
- Aspinall, G. O. & Cottrell, I. W. Polysaccharides of soybeans. VI. Neutral polysaccharides from cotyledon meal. *Can. J. Chem.* **49**, 1019–1022 (1971).
- Tett, A. et al. The *Prevotella copri* complex comprises four distinct clades underrepresented in westernized populations. *Cell Host Microbe* **26**, 666–679 (2019).
- Vatanen, et al. A distinct clade of *Bifidobacterium longum* in the gut of Bangladeshi children thrives during weaning. *Cell* **185**, 4280–4297 (2022).
- Fujita, K. et al. Degradative enzymes for type II arabinogalactan side chains in *Bifidobacterium longum* subsp. *longum*. *Appl. Microbiol. Biotechnol.* **103**, 1299–1310 (2019).
- Komeno, M., Hayamizu, H., Fujita, K. & Ashida, H. Two novel α -L-arabinofuranosidases from *Bifidobacterium longum* subsp. *longum* belonging to glycoside hydrolase family 43 cooperatively degrade arabinan. *Appl. Environ. Microbiol.* **85**, e02582 (2019).
- Barratt, M. J. et al. *Bifidobacterium longum* subsp. *infantis* strains for treating severe acute malnutrition in Bangladeshi infants. *Sci. Trans. Med.* **14**, 640 (2022).
- Terrapon, N., Lombard, V., Gilbert, H. J. & Henrissat, B. Automatic prediction of polysaccharide utilization loci in Bacteroidetes species. *Bioinformatics* **31**, 647–655 (2015).
- Terrapon, N. et al. PULDB: the expanded database of Polysaccharide Utilization Loci. *Nucleic Acids Res.* **46**, D677–D683 (2018).
- Palackal, N. et al. A multifunctional hybrid glycosyl hydrolase discovered in an uncultured microbial consortium from ruminant gut. *Appl. Microbiol. Biot.* **74**, 113–124 (2007).
- McGregor, N. et al. Structure-function analysis of a mixed-linkage β -glucanase/xyloglucanase from the key ruminal Bacteroidetes *Prevotella bryantii* B14. *J. Biol. Chem.* **291**, 1175–1197 (2016).
- Fehlner-Peach, H. et al. Distinct polysaccharide utilization profiles of human intestinal *Prevotella copri* isolates. *Cell Host Microbe* **26**, 680–690 (2019).
- Chang, H.-W. et al. *Prevotella copri*-linked effects of a therapeutic food for malnutrition. Preprint at bioRxiv <https://doi.org/10.1101/2023.08.11.553030> (2023).

Publisher’s note Springer Nature remains neutral with regard to jurisdictional claims in published maps and institutional affiliations.



Open Access This article is licensed under a Creative Commons Attribution 4.0 International License, which permits use, sharing, adaptation, distribution and reproduction in any medium or format, as long as you give appropriate credit to the original author(s) and the source, provide a link to the Creative Commons licence, and indicate if changes were made. The images or other third party material in this article are included in the article’s Creative Commons licence, unless indicated otherwise in a credit line to the material. If material is not included in the article’s Creative Commons licence and your intended use is not permitted by statutory regulation or exceeds the permitted use, you will need to obtain permission directly from the copyright holder. To view a copy of this licence, visit <http://creativecommons.org/licenses/by/4.0/>.

© The Author(s) 2023

Methods

Collection and handling of biospecimens obtained from participants in the randomized controlled clinical study of the efficacy of MDCF-2

The human study entitled 'Community-based clinical trial with microbiota-directed complementary foods (MDCFs) made of locally available food ingredients for the management of children with primary moderate acute malnutrition (MAM)' was approved by the Ethical Review Committee at the icddr,b (protocol PR-18073; ClinicalTrials.gov: NCT04015999)⁴. Informed consent was obtained for all of the participants. The objective of the study was to determine whether twice daily, controlled administration of a locally produced, microbiota-directed complementary food (MDCF-2^{3,4}) for 3 months to children with MAM provided superior improvements in weight gain, microbiota repair and improvements in the levels of key plasma biomarkers/mediators of healthy growth, compared with a commonly used rice- and lentil-based RUSF formulation.

A total of 124 male and female children with MAM (WLZ, -2 to -3) between 12- and 18-months old who satisfied the inclusion criteria were enrolled, with 62 children randomly assigned to each treatment group using the permuted block randomization method. Children in each treatment group were fed their assigned dietary supplement (MDCF-2 or RUSF) twice daily at a study centre for the first month, once daily at a study centre and once daily at home for the second month, and twice daily at home for the third month. Mothers were otherwise encouraged to practice their customary breast-feeding and complementary-feeding practices. At the end of the intervention period, children returned to their normal feeding routine with continued intensive monitoring for one additional month. Fifty-nine participants in each treatment group completed the 3-month intervention and 1-month post-treatment follow-up⁴.

To minimize the risk of degradation of faecal DNA/RNA, faecal samples were collected within 20 min of their production and immediately transferred to liquid-nitrogen-charged vapour shippers for transport to a -80 °C freezer at the study centre. The samples were shipped to Washington University on dry ice where they were stored at -80 °C in a dedicated repository with approval from the Washington University Human Research Protection Office.

MAGs

Short-read shotgun sequencing. DNA was isolated from 942 faecal samples as previously described⁴ and shotgun sequencing libraries were prepared using a reduced-volume Nextera XT (Illumina) protocol³⁰. Libraries were quantified, balanced, pooled and sequenced (Illumina NovaSeq 6000, S4 flow cell; $2.3 \pm 1.4 \times 10^7$ 150-nucleotide paired-end reads/sample (mean \pm s.d.)). Reads were demultiplexed (bcl2fastq, Illumina), trimmed to remove low-quality bases and processed to remove read-through adapter sequences (Trim Galore³¹, v.0.6.4). Read pairs for which the length of either read was <50 nucleotides after quality and adapter trimming were discarded. The remaining reads were mapped to the human genome (UCSC hg19) using bowtie2³² (v.2.3.4.1) and were subsequently filtered to remove *Homo sapiens* sequences.

Preprocessed, short-read shotgun data were aggregated from each participant's faecal sample set ($n = 7-8$ samples per participant; 118 participants) before MAG assembly. This strategy was adopted to enable the contig abundance calculations required by the MAG assembly algorithms used below, while at the same time mitigating the risk of chimeric assemblies inherent to co-assembly across individuals. Assemblies were generated for all 118 datasets using MegaHit³³ (v.1.1.4), and the resulting contigs were quantified in each assembly by mapping preprocessed reads to the assembled contigs using kallisto³⁴. Contigs were assembled into MAGs using MaxBin2³⁵ (v.2.2.5) and MetaBAT2³⁶ (v.2.12.1). The parallel results of both binning

strategies were merged and dereplicated using DAS Tool³⁷ (v.1.1.2) on a per-participant basis.

Long-read shotgun sequencing. We applied long-read sequencing to faecal samples obtained at the 0- and 3-month timepoints from each of the 15 upper-quartile WLZ responders in the MDCF-2 treatment group. Aliquots containing 400–1,000 ng of DNA from each biospecimen were transferred to a 96-well, 0.8 ml, deep-well plate (Nunc, Thermo Fisher Scientific) and prepared for long-read sequencing using the SMRTbell Express Template Prep Kit 2.0 (PacBio). All subsequent DNA handling and transfer steps were performed with wide-bore, genomic DNA pipette tips (ART, Thermo Fisher Scientific). Barcoded adapters were ligated to A-tailed DNA fragments by overnight incubation at 20 °C. Adapter-ligated fragments were then treated using the SMRTbell Enzyme Cleanup Kit to remove damaged or partial SMRTbell templates. A high molecular mass DNA fraction was purified using AMPure beads (ratio of 0.45 \times well-mixed AMPure bead volume to sample) and eluted in 12 μ l of PacBio elution buffer. DNA libraries were sequenced on the Sequel System (Pacific Biosciences) using the Sequel Binding Kit 3.0 and Sequencing Primer v4 with 24 h of data collection. A total of $3.0 \times 10^9 \pm 9.8 \times 10^8$ bp per sample were collected, with an average subread length of $5,654 \pm 871$ bp (mean \pm s.d.).

Hybrid assembly of short- and long-read data was performed using OPERA-MS³⁸ (v.0.9.0). OPERA-MS uses assembly graph and coverage-based methods to cluster contigs into MAGs based on optimizing per-cluster Bayesian information criterion. Before hybrid assembly, continuous long reads (CLRs) were combined across the two available timepoints for each participant and reads that mapped to the human genome were removed. Illumina short reads and PacBio long reads (CLRs) were provided to OPERA-MS and assembled using the built-in OPERA-MS genome database and the default settings (the latter includes polishing of output MAGs with Pilon³⁹).

MAG dereplication, curation and abundance calculations. After assembling MAGs using both the short-read-only and short-read plus long-read strategies, all MAGs from all assembly strategies were assessed for completeness and contamination ('lineage_wf' command in CheckM⁴⁰, v.1.1.3) and refined ('tetra', 'outliers' and 'modify' commands in CheckM) to remove contaminating contigs. Additional refinement based on the distribution of phylogenetic markers present in each MAG was performed ('phylo-markers', 'clade-markers' and 'clean-bin' commands in MAGpurify⁴¹ (v.2.1.2)). A final MAG quality assessment was performed using CheckM, followed by a stringent ($\geq 90\%$ complete, $\leq 5\%$ contaminated, average nucleotide identity (ANI) $\geq 99\%$) bulk dereplication across all MAGs from all of the participants (options '-l 50000', '--completeness 90', '--contamination 5', '-pa 0.9', '-sa 0.99' in dRep⁴² (v.2.6.2)). The final dataset contained 681 ± 99 (mean \pm s.d.) MAGs per participant. MAG assembly summary statistics were collected from CheckM⁴⁰ and quast⁴³ analyses (v.4.5) and aggregated (Supplementary Table 1 and Extended Data Fig. 10). Initial MAG annotations were performed using prokka⁴⁴ (v.1.14.6). Further details about benchmarking the methods we used for assembly are presented in the Supplementary Discussion. To quantify the abundance of each MAG in each sample, MAGs were processed to create a single kallisto quantification index⁴⁵. Reads from each faecal DNA sample were then mapped to this index.

MAG taxonomy. Taxonomic assignments were initially made using the Genome Taxonomy Database Toolkit¹⁵ (GTDB-Tk) and the corresponding database (release 95). We complemented these MAG assignments using Kraken2⁴⁶ (v.2.0.8) and Bracken⁴⁷ (v.2.5) and a Kraken2-compatible version of the GTDB reference.

P. copri has been partitioned into four distinct clades (A–D) on the basis of marker gene phylogeny¹⁹. To classify *Prevotella* MAGs in this study, we constructed an unrooted, marker-gene-based phylogeny

using PhyloPhlan⁴⁸ (v.3.0.60). This tree encompassed 17 reference isolate genomes and 1,006 MAGs from a previous study¹⁹ plus any MAGs from our set classified by GTDB-Tk as belonging to the genera *Prevotella* ($n = 51$) or *Prevotellamassilia* ($n = 13$). Putative *Prevotella* MAGs from the present study that clustered within the four previously identified *P. copri* clades were assigned to the corresponding clade based on visualization using Graphlan⁴⁹ (v.1.1.4).

Certain *Bifidobacterium* species consist of multiple closely related subspecies (such as *B. longum*). We therefore calculated a pan-genome for 34 *Bifidobacterium* MAGs in our dataset (Supplementary Table 1), plus 14 reference isolate genomes (Supplementary Fig. 5), using Roary⁵⁰ (v.3.12.0) and a 60% minimum sequence identity threshold for BLASTp⁵¹. The reference isolate genomes included ten *Bifidobacterium* species and three subspecies of *B. longum* (ssp. *longum*, *infantis* and *suis*). Concatenated nucleotide sequences of 142 identified core genes were aligned using MAFFT⁵² (v.7.313). The resulting alignment was trimmed (microseq⁵³ R package (v.2.1.4)) and then used to construct a maximum-likelihood phylogenetic tree (IQ-TREE⁵⁴ (v.1.6.12)). The *B. gallicum* DSM 20093 genome was selected as an outgroup. Putative *Bifidobacterium* MAGs from this study that clustered together with reference genome clades were assigned to the corresponding clade. Using this method, we were able to confirm or update our initial GTDB-Tk-based classifications of all *Bifidobacterium* MAGs and resolve nearly all closely related subspecies (Supplementary Table 1 and Supplementary Fig. 5).

Defining the relationship between MAG abundances and WLZ

The procedures used for shotgun sequencing of faecal DNA and pre-processing of the resulting reads, plus MAG assembly and quantification are described in the Methods.

Linear mixed-effects models were used to relate the abundances of MAGs identified in each trial participant to WLZ using the formula:

$$WLZ - \beta_1(\text{MAG}) + \beta_2(\text{study week}) + (1 | \text{PID})$$

Our data normalization strategies before linear modelling did not include a consideration of MAG assembly length. We therefore analysed the TPM (reads per kilobase per million) output of kallisto (v.0.43.0) by applying a filter requiring each MAG's abundance to be >5 TPM in >40% of the 707 faecal samples collected at timepoints at which anthropometry was also measured. This filtering approach yielded 837 MAGs. We then returned to the unfiltered count output from kallisto, performed a variance-stabilizing transformation (VST, DESeq2⁵⁵ (v.1.34.0)) to control for heteroskedasticity, and filtered the dataset to the same 837 MAGs. We subsequently fit linear mixed-effects models to the transformed abundances of each MAG across all 707 faecal samples (lme4⁵⁶, v.1.1-27.1; lmerTest⁵⁷, v.3.1-3). We used analysis of variance to determine the statistical significance of the fixed effects in our model—specifically, the relationship between MAG abundance and WLZ. WLZ-associated MAGs were defined as those with false-discovery-rate-adjusted $P(q) < 0.05$.

Determining the effects of MDCF-2 supplementation on the abundances of WLZ-associated MAGs

We used dream⁵⁸ (variancePartition R package, v.1.24.0) an empirical Bayesian linear mixed-effects modelling framework, to model MAG abundance as a function of treatment group, study week and their interaction, controlling for the repeated measurements taken from each study participant with a random effect term for participant. The equation used to quantify the effects of treatment on MAG abundance took the form:

$$\text{MAG}_i - \beta_1(\text{treatment group}) + \beta_2(\text{study week}) + \beta_3(\text{treatment group} \times \text{study week}) + (1 | \text{PID})$$

The 'treatment group' coefficient β_1 indicates whether MDCF-2 produced changes in the mean abundance of a given MAG relative to RUSF over the 3-month intervention, whereas the 'treatment group \times study week' interaction coefficient β_3 indicates whether MDCF-2 affected the rate of change of a given MAG more so than RUSF (that is, whether a MAG increases or decreases more rapidly in the microbiomes of participants in the MDCF-2- versus the RUSF-treatment group). Each coefficient for each MAG abundance analysis is described by an associated t -statistic—a standardized measure, based on standard error, of a given coefficient's deviation from zero that can be used to calculate a P value and infer the significance of the effect of a given coefficient on the dependent variable. The t -statistics produced using this method can also be used as a ranking factor for input into GSEA. For this analysis, gene sets were defined as groups of MAGs that were either significantly positively ($n = 75$) or significantly negatively ($n = 147$) associated with WLZ. This analysis was conducted for both the 'treatment group' (β_1) coefficient and the 'treatment group \times study week' interaction (β_3) coefficient. Statistical significance is reported as q values after adjustment for false-discovery rate (using the Benjamini–Hochberg method).

Microbial RNA-seq analysis of MAG gene expression

For RNA extraction, approximately 50 mg of a faecal sample, collected from each participant at the baseline, 1-month and 3-month timepoints, was pulverized under liquid nitrogen with a mortar and pestle and aliquoted into 2 ml cryotubes. A 3.97 mm steel ball and 250 μ l of 0.1 mm zirconia/silica beads were subsequently added to each sample tube, together with 500 μ l of a mixture of phenol:chloroform:isoamyl alcohol (25:24:1, pH 7.8–8.2), 210 μ l of 20% SDS and 500 μ l of 2 \times Qiagen buffer A (200 mM NaCl, 200 mM Trizma base, 20 mM EDTA). After a 1 min treatment in a bead beater (Biospec Minibeadbeater-96), the samples were centrifuged at 3,220g for 4 min at 4 °C. Then, 100 μ l of the resulting aqueous phase was transferred by a liquid-handling robot (Tecan) to a deep 96-well plate along with 70 μ l of isopropanol and 10 μ l of 3 M NaOAc, pH 5.5. The solution was mixed by pipetting ten times. The crude DNA/RNA mixture was incubated at –20 °C for 1 h and then centrifuged at 3,220g at 4 °C for 15 min before removing the supernatant to yield nucleic-acid-rich pellets. A Biomek FX robot was used to add 300 μ l Qiagen buffer RLT to the pellets and to resuspend the RNA/DNA by pipetting up and down 50 times. A 400 μ l aliquot was transferred from each well to an Qiagen AllPrep 96 DNA plate, which was centrifuged at 3,220g for 1 min at room temperature. The RNA flow-through was purified as described in the AllPrep 96 protocol. cDNA libraries were prepared from extracted RNA using an Illumina Total RNA Prep with Ribo-Zero Plus and dual unique indexes. Libraries were balanced, pooled and sequenced in two runs of an Illumina NovaSeq using S4 flow cells.

As an initial pre-processing step, raw reads were aggregated by sample across the two NovaSeq runs, resulting in a total of $5.0 \times 10^7 \pm 4.7 \times 10^6$ paired-end 150-nucleotide reads per sample (mean \pm s.d.). Adapter sequences and low-quality bases were removed from raw reads (Trim Galore³¹, v.0.6.4), and pairs of trimmed reads were filtered out if either one of the paired reads was less than 100 nucleotides long. Pre- and post-trimmed sequence quality and adapter contamination were assessed using FastQC⁵⁹ (v.0.11.7). Filtered reads were pseudoaligned to the set of 1,000 annotated, dereplicated high-quality MAGs to quantify transcripts with kallisto³⁴. Reads that pseudoaligned to rRNA genes were excluded, leaving an average of $7.1 \times 10^6 \pm 3.9 \times 10^6$ bacterial mRNA reads (mean \pm s.d.) per sample. Count tables were further filtered to retain only transcripts that pseudoaligned to the 837 MAGs that passed the abundance and prevalence thresholds described above. To minimize inconsistently quantified counts related to low-abundance MAGs, we assigned a transcript count of zero, on a per-sample basis, to any MAG with a DNA abundance < 0.5 TPM in that sample.

Differential expression analysis (edgeR⁶⁰, v.3.32.1) was conducted using the following steps: (1) transcript filtering for presence/absence

Article

and prevalence; (2) library-size normalization using trimmed mean of M values (TMM); (3) estimating per-gene count dispersions; and (4) testing for differentially expressed genes. Transcripts were first filtered using the edgeR default parameters, followed by a parameter sweep of transcript abundance and prevalence threshold combinations. On the basis of this analysis, transcripts with ≥ 5 counts per million mapped reads in $\geq 35\%$ of samples were retained for differential expression analysis. The transcripts that passed this filtering were normalized using a TMM-based scaling factor. We next estimated negative binomial dispersions and fit trended per-gene dispersions (using the power method) to negative binomial generalized linear models. These models were used to characterize (1) the effect of treatment group and study week among all participants and (2) the effect of WLZ quartile and study week among MDCF-2 participants in the upper and lower quartiles of WLZ response using the following model formula:

$$\begin{aligned} & \text{transcript}_i - \beta_1(\text{treatment group}) + \beta_2(\text{study week}) \\ & \quad + \beta_3(\text{treatment group} \times \text{study week}) \\ & \text{transcript}_i - \beta_1(\text{WLZ-response quartile}) + \beta_2(\text{study week}) \\ & \quad + \beta_3(\text{WLZ-response quartile} \times \text{study week}) \end{aligned}$$

From these models, we identified genes that exhibited significant differential expression using the quasi-likelihood F -test (edgeR, function `glmQLFTest`), which accounts for the uncertainty in estimating the dispersion for each gene.

For subsequent functional metabolic pathway enrichment analyses, we (1) ordered transcripts assigned to WLZ-associated MAGs on the basis of a ranking metric calculated as the direction of the fold-change $\times -\log_{10}[P]$ for a given differential expression analysis; (2) defined gene sets as groups of these ranked transcripts assigned to the same metabolic pathway; and (3) performed GSEA (`fgsea`⁶¹, v.3.14). This set of analyses enabled us to identify differentially expressed metabolic pathways comprised of ≥ 10 genes over time (1) between treatment groups; (2) between WLZ-response quartiles; or (3) as a function of interacting terms in the linear mixed effect models (treatment group \times study week; WLZ-response quartile \times study week). Enrichment results were considered to be statistically significant if they exhibited $q < 0.1$ after controlling for false-discovery rate (Benjamini–Hochberg method).

For targeted transcriptional analyses of the CAZymes encoded by *P. copri* MAGs Bg0018 and Bg0019, we used `dream`⁵⁸ in R with no additional filtering, and the formula above relating transcripts to WLZ response quartile, study week and the interaction of both terms, with the addition of a random effect for participant.

PCA

PCA was performed on VST-transformed DNA or transcript counts for the 837 MAGs passing the filter described in the 'Defining the relationship between MAG abundances and WLZ' section above. The PCA performed on transcript abundances encompassed 27,518 genes expressed by these MAGs at thresholds for levels and prevalence that are described in the 'Microbial RNA-seq analysis of MAG gene expression' section above. PCA was performed in R using the 'prcomp' function, with each data type centred but not scaled as the dataset was already VST-normalized. The functions 'get_eigenvalues', 'get_pca_ind' and 'get_pca_var' from the `factoextra`⁶² (v.1.0.7) package were used to extract (1) the variance explained by each PC; (2) the coordinates for each sample along PCs; and (3) the contributions of each variable to PC1–3. We used the 'adonis2' function within the `vegan`⁶³ library (v.2.5-7) to test for the statistical significance of differences in the microbiome (MAGs) or metatranscriptome between the two treatment groups at baseline or over time.

LC-MS analyses of carbohydrates present in MDCF-2, RUSF, their component ingredients, faecal specimens and culture medium

Sample preparation for glycan structure analysis. Frozen samples of MDCF-2, RUSF, their respective ingredients and faecal biospecimens were ground with a mortar and pestle while submerged in liquid nitrogen. A 50 mg aliquot of each homogenized sample was lyophilized to dryness. Lyophilized samples were shipped to the Department of Chemistry at the University of California, Davis. On receipt, the samples were pulverized to a fine powder using 2 mm stainless-steel beads (for foods) or 2 mm glass beads (for faeces). A 10 mg ml⁻¹ stock solution of each sample was prepared in Nanopure water. All stock solutions were again bead homogenized, incubated at 100 °C for 1 h, bead homogenized again and stored at -20 °C until further analysis.

Monosaccharide composition analysis. Methods were adapted from previous publications^{64,65}. For analyses of food ingredients and faecal biospecimens, 10 μ l aliquots were withdrawn from homogenized stock solutions and transferred to a 96-well plate containing 2 ml wells. For analyses of monocultures of *P. copri* strains grown in the presence of different purified polysaccharides, microplates were withdrawn from anaerobic chamber at the conclusion of the incubation and centrifuged (5,000g for 5 min). The resulting supernatants were removed and immediately frozen at -80 °C.

Each sample was subjected to acid hydrolysis (4 M trifluoroacetic acid for 1 h at 121 °C) followed by addition of 855 μ l of ice-cold Nanopure water. Hydrolysed samples, plus an external calibration standard comprising 14 monosaccharides with known concentrations (0.001–100 μ g ml⁻¹ each) were derivatized with 0.2 M 1-phenyl-3-methyl-5-pyrazolone (PMP) in methanol plus 28% NH₄OH for 30 min at 70 °C. The derivatized glycosides were fully dried by vacuum centrifugation, reconstituted in Nanopure water (Thermo Fischer Scientific) and excess PMP was extracted with chloroform. A 1 μ l aliquot of the aqueous layer was injected into the Agilent 1290 Infinity II ultrahigh-performance liquid chromatography (UHPLC) system, separated using a 2 min isocratic elution on a C18 column (Poroshell HPH, 2.1 \times 50 mm, 1.9 μ m particle size, Agilent Technologies) and analysed using the Agilent 6495A triple quadrupole mass spectrometer (QqQ-MS) operated in dynamic multiple-reaction-monitoring mode. Monosaccharides in the food and faecal samples were identified and quantified by comparison to the external calibration curve.

Glycosidic linkage analysis. Methods were adapted from a previous publication with modifications^{66,67}. Under an argon atmosphere, a 5 μ l aliquot from each homogenized stock solution of a sample was permethylated in a 200 μ l reaction that contained 5 μ l saturated NaOH and 40 μ l iodomethane in 150 μ l of DMSO. Permethylated glycosides were extracted with dichloromethane, and the extract was dried by vacuum centrifugation. The extracted glycosides were processed for acid hydrolysis (4 M trifluoroacetic acid for 2 h at 100 °C) followed by vacuum centrifugation to dryness. The samples were then derivatized with PMP as described above for monosaccharide analysis, followed by another vacuum centrifugation to complete dryness. Methylated monosaccharides were then reconstituted with 100 μ l of 70% methanol in water. A 1 μ l aliquot of the aqueous layer was injected into the Agilent 1290 Infinity II UHPLC system, separated using a 16 min gradient elution on a C18 column (ZORBAX RRHD Eclipse Plus, 2.1 \times 150 mm, 1.8 μ m particle size, Agilent Technologies), and analysed using the Agilent 6495A QqQ-MS operated in multiple-reaction-monitoring mode. A standard pool of oligosaccharides and a reference MRM library were used to identify and quantify glycosidic linkages in all of the samples.

FITDOG polysaccharide analysis. Methods were adapted from previous publications^{17,68}. To separate endogenous oligosaccharides from the background food matrix, polysaccharides were precipitated with

80% aqueous ethanol. Dried precipitates were reconstituted in water to 10 mg ml⁻¹ and then homogenized. The Fenton's initiation toward defined oligosaccharide groups (FITDOG) reaction was performed using a 100 µl aliquot of the 10 mg ml⁻¹ resuspended food pellet and 900 µl of reaction buffer (44 mM sodium acetate, 1.5% H₂O₂, 73 µM Fe₂(SO₄)₃(H₂O)₅). The reaction mixture was incubated at 100 °C for 45 min, quenched with 500 µl 2 M NaOH and then neutralized with 61 µl of glacial acetic acid. The resulting oligosaccharides were then reduced to their corresponding alditols with sodium borohydride (NaBH₄) to prevent anomerization during chromatographic separation. For the reduction of oligosaccharides, a 400 µl aliquot of the reaction mixture was incubated with 400 µl 1 M NaBH₄ at 65 °C for 60 min. Oligosaccharide products were then enriched using C18 and porous graphitized carbon (PGC) 96-well solid-phase extraction plates. For the C18 enrichment, cartridges were primed with two washes with 250 µl acetonitrile and then five washes with 250 µl water washes before loading the reduced sample. The cartridge effluent was collected and processed for subsequent PGC clean-up. PGC cartridges were primed with 400 µl water, 400 µl 80% acetonitrile/0.1% (v/v) trifluoroacetic acid, and then 400 µl water before loading the C18 effluent. Washing was performed with 8 × 400 µl water, and the oligosaccharides were eluted with 40% acetonitrile/0.05% (v/v) trifluoroacetic acid and then dried using a vacuum centrifugal dryer. Oligosaccharides were reconstituted with 100 µl Nanopure water and a 10 µl aliquot was injected into the HPLC-Q-TOF instrument. Separation was performed using the Agilent 1260 Infinity II HPLC system with a PGC column (Hypercarb, 1 × 150 mm, 5 µm particle size, Thermo Fisher Scientific) coupled to the Agilent 6530 Accurate-Mass Q-TOF mass spectrometer. Specific HPLC, electrospray source and MS acquisition parameters are described in greater detail in previous publications^{17,68}. Oligosaccharide identification was based on MS/MS fragmentation and retention time compared to reacted polysaccharide standards (amylose, cellulose, mannan, galactan, linear arabinan and xylan). Food polysaccharides were quantified using an external calibration curve that included the three most abundant oligosaccharides from each parent polysaccharide as the quantifier species.

Statistical analysis of carbohydrate composition. We analysed the abundances of glycosidic linkages over time and between WLZ-response quartiles using linear mixed-effects models (lme4⁵⁶, lmerTest⁵⁷ packages in R) of the following form:

$$\text{linkage}_i \sim \beta_1(\text{WLZ-response quartile}) + \beta_2(\text{study week}) \\ + \beta_3(\text{WLZ-response quartile} \times \text{study week}) + (1|\text{PID})$$

Linkages displaying a significant interaction ($q < 0.05$) between WLZ-response quartile and study week (β_3 coefficient) were identified.

Culturing *P. copri* from faecal samples and genome sequencing

Faecal samples, obtained from our previously reported studies of Bangladeshi children living in Mirpur^{3,4}, were first screened on the basis of the abundances of *P. copri* V4-16S rDNA amplicon sequence variants and/or *P. copri* MAGs. Five samples from our previous pilot MDCF study³, plus an additional 32 samples from the larger randomized controlled clinical trial (prioritized on the basis of participants' membership in the upper quartile of WLZ response to MDCF-2 treatment) were selected for this culturing effort.

A frozen aliquot (~0.1 g) of each selected faecal sample was weighed. All of the subsequent steps were performed under anaerobic conditions (atmosphere: 75% N₂, 20% CO₂, 5% H₂) in a Coy chamber (Coy Laboratory Products). For the faecal samples that yielded strains BgD5_2, BgF5_2 and BgG5_1, aliquots were resuspended directly in 100 µl of phosphate-buffered saline (PBS) containing 0.5% (w/v) L-cysteine. All of the other samples were clarified as described previously³. A 100 µl aliquot of each resuspended or clarified sample was serially diluted

in PBS containing 0.5% (w/v) L-cysteine and plated onto Laked sheep blood-kanamycin-vancomycin agar plates (Hardy Diagnostics, A60). *Prevotella* spp. produce a pigment known to fluoresce brick red when exposed to ultraviolet light. Thus, colonies grown from serial dilutions were screened for this phenotype, picked and struck onto brain-heart infusion (BHI, Difco, 241830) agar plates containing 10% horse blood. Individual isolated colonies were picked into liquid Wilkins-Chalgren medium (Oxoid, CM0643), grown overnight at 37 °C and then mixed 1:1 with prereduced 30% glycerol (in PBS plus 0.5% (w/v) L-cysteine) in 1.8 ml glass vials (E-Z vials, Wheaton). Vials were closed by crimping on a cover containing a PTFE/grey butyl liner (Wheaton). Stocks were preserved at -80 °C for later use. An additional aliquot of each culture was processed for full-length 16S rDNA sequencing (universal primers 8F and 1391R) to provide an initial taxonomic identification. This effort yielded a total of 108 isolates assigned to *Prevotella* spp., including 86 classified as *P. copri*.

Each *P. copri* isolate was retrieved from storage, cultured in Wilkins-Chalgren medium and processed for whole-genome sequencing. Freezer stocks of each bacterial isolate were inoculated into Wilkins-Chalgren medium and grown at 37 °C under anaerobic conditions without shaking until reaching late-log phase. A 6 ml aliquot of each culture was withdrawn from the anaerobic chamber and centrifuged at 5,000g for 5 min. The resulting cell pellet (10–50 mg) was transferred to a 2 ml cryotube and DNA was extracted by bead beating (Biospec Minibeadbeater-96) for 1 min with a 3.97 mm steel ball and 250 µl of 0.1 mM zirconia/silica beads in 500 µl of 25:24:1 phenol:chloroform:isoamyl alcohol solution, 210 µl of 20% SDS and 500 µl of 2× buffer A (200 mM NaCl, 200 mM Trizma base, 20 mM EDTA)⁶⁹. The resulting mixtures were centrifuged at 3,220g for 4 min at 22 °C. A 420 µl aliquot of the resulting aqueous phase was transferred to a deep 96-well plate and purified using the QIAquick 96-well PCR purification kit (Qiagen). DNA was quantified (Quant-iT dsDNA broad range kit; Invitrogen) and the fragment-size distribution was measured (TapeStation using a genomic DNA ScreenTape (Agilent)).

Purified DNA was prepared for long-read sequencing using the SMRTbell Express Template Prep Kit 2.0 from Pacific Biosciences (Pacific Biosciences; PacBio); we followed the manufacturer's instructions for creating HiFi Libraries from low DNA input, with adjustments made to accommodate a 96-well plate configuration⁶⁹. The DNA concentration and fragment-size distribution of resulting libraries were evaluated (genomic DNA ScreenTape; TapeStation instrument) and the libraries were pooled at equimolar concentrations after normalizing for expected genome size. Pooled libraries were sequenced on the Sequel long-read DNA sequencer (PacBio) using the Sequel Binding Kit 3.0 and Sequencing Primer v4, with 24 h of data collection. The samples were demultiplexed, and Q20 circular consensus sequencing reads were generated using the Cromwell workflow from PacBio. The Flye⁷⁰ assembler (v.2.8.1) was used to assemble the genomes, with the HiFi-error set to 0.003, min-overlap set at 2000 and other options kept as the default. Genome quality was evaluated using CheckM⁴⁰ (v.1.1.3), and genomes were annotated using prokka⁴⁴ (v.1.14.6).

Constructing a marker-gene-based phylogeny for *P. copri* MAGs and cultured *P. copri* isolates

We used CheckM⁴⁰ (v.1.1.3) to extract and align the amino acid sequences of 43 single-copy marker genes in each of the 11 *P. copri* MAGs, each of the 6 cultured *P. copri* strains, plus the type strain of *Bacteroides thetaiotaomicron* VPI-5482 (accession number: 226186.12). Concatenated, aligned marker gene sequences were analysed (fasttree⁷¹; v.2.1.10) using the Jones-Taylor-Thornton model and 'CAT' evolution rate to create a phylogenetic tree, which was subsequently rescaled using the 'Gamma20' optimization. The resulting tree was rooted to the *B. thetaiotaomicron* genome ('ape', v.5.6-2⁷²) before extracting the phylogenetic distances between MAGs and isolates. The tree was visualized using ggtree⁷³ (v.3.2.1).

Subsystem-based annotation and prediction of functional capabilities (inferred metabolic phenotypes) of MAGs and cultured *P. copri* strains

MAG and isolate genes were assigned functions, and metabolic pathways were reconstructed using a combination of (1) public-domain tools for sequence alignment and clustering; (2) custom scripts to process the results of sequence alignments (for example, for domain annotation in multifunctional proteins); and (3) a reference collection of 2,856 human gut bacterial genomes for which we have reconstructed and manually curated metabolic pathways related to 98 distinct metabolites and 106 metabolic phenotypes¹⁶. These annotations are captured in the mcSEED database, a microbial community-centred adaptation of the SEED genomic platform^{14,15}, featuring subsystem-based annotation and pathway reconstruction applied to representative human gut bacterial genomes that were initially automatically annotated by RAST or downloaded from the PATRIC (recently renamed Bacterial and Viral Bioinformatic Resource Center, BV-BRC) database⁷⁴. Each mcSEED subsystem includes a set of functional roles (for example, enzymes, transporters, transcriptional regulators) that contribute to the prediction of functional metabolic pathways and pathway variants⁷⁵ that are involved in the utilization and catabolism of carbohydrates and amino acids, biosynthesis of vitamins/cofactors and amino acids, and generation of fermentation end-products such as short-chain fatty acids. A complete list of MAG genes comprising these pathways, their abbreviations and functions is provided in Supplementary Table 5 (annotations are based on the January 2021 version of the mcSEED database).

Our annotation workflow is shown in Supplementary Fig. 1. In brief, we constructed a reference database containing 995,591 functionally annotated proteins comprising the entire set of curated metabolic subsystems from the 2,856 reference genomes plus an additional 2,988,751 proteins (outgroup is not included in these metabolic subsystems), clustered at 90% amino acid identity ('cluster' command, MMSeqs⁷⁶, v.1-c7a89). We aligned the predicted protein sequences from the set of 1,000 high-quality MAGs against this reference protein database (DIAMOND⁷⁷, v.2.0.0). To account for any influence of MAG fragmentation on metabolic reconstruction, we also identified gene fragments using prodigal⁷⁸ (v.2.6.3) and annotated them in parallel. We implemented the following method to account for instances of multidomain structure that require multiple annotations. For each MAG query protein, we used the top 50 hits based on the bitscore, clustered the start and end position coordinates of the corresponding alignments (DBSCAN function, Scikit-learn^{79,80}, v.0.22.1), used the centre of each clustered start and end position as potential domain boundary coordinates, and split query proteins into domains with database hits attributed to the corresponding domains. Next, for each domain of ≥ 35 amino acids, we used Gaussian kernel density modelling (KernelDensity function, neighbours module, Scikit-learn⁸⁰) of the sequence identity distribution of each set of hits to that domain. A highest local minimum (argrextrema function, signal module, Scikit-learn⁸⁰) was used as a threshold to remove low-confidence hits. Finally, functional annotations were applied from the reference database to each query protein or domain by majority rule within each set of high-scoring, domain-specific reference hits. High-identity hits to proteins from the outgroup of the reference database were used as criteria to vote against applying annotation to each query. This procedure yielded a set of 199,334 annotated MAG proteins, representing 1,308 unique protein products across a set of 80 mcSEED subsystems (Supplementary Table 5).

Phenotype prediction strategies. We integrated the results of gene-level functional annotation into *in silico* predictions of the presence or absence (denoted as binary: '1' for presence or '0' for absence) of 106 functional metabolic pathways (Supplementary Table 7) using a semi-automated process based on a combination of the following three approaches:

Pathway-rules-based phenotype predictions. This approach uses explicit logic-based 'pathway rules' to assign binary phenotypes. These rules combine (1) expert curators' knowledge regarding the gene composition of various metabolic pathway variants contained in the mcSEED database with (2) a decision tree method to identify patterns of gene representation in reference genomes corresponding to an intact functional pathway variant (and a respective binary phenotype value denoted as '1'). A total of 106 functional pathway-specific decision trees was generated (Rpart⁸¹, v.4.1.15), where the presence or absence of a particular phenotype was the response variable, and the presence or absence of functional roles (encoded by genes) in each reference pathway were predictor variables. The resulting pathway rules were formally encoded into a custom R script that enabled us to process MAG gene data and assign values (1 or 0) for each of the 106 functional metabolic pathways.

Machine-learning-based phenotype predictions. We compared >30 ml methods (Caret⁸², v.6.0.86), using a leave-one-out cross-validation approach in which we removed a single reference genome from the set of 2,856 reference genomes, trained machine-learning models on the remaining genomes, then applied the models to the 'test' genome to predict phenotypes. This procedure was then repeated for each genome and each metabolic phenotype. The results of this analysis identified random forest as the best-performing method (that is, it produced the greatest number of correctly predicted phenotypes in our reference training dataset). We then built random-forest models for each phenotype based on the reference dataset, optimized model parameters using a grid search and used these models to predict binary (1/0) values for the same set of 106 phenotypes for all MAGs.

Neighbour-group-based phenotype predictions. This approach identifies reference bacteria that are closely related to the MAGs in this study and uses these high-quality reference genomes for phenotype predictions that are robust to variation in MAG quality. Examination of groups of closely related reference organisms suggested that close phylogenetic neighbour genomes tend to either possess or lack an entire pathway variant, whereas more distant neighbours (such as other neighbour groups) often carry more divergent pathway variants that specify the same phenotype. We used this observation to develop heuristics that minimize false-negative phenotype assignments emerging from the other two prediction strategies. We compiled a set of neighbour groups comprising MAGs and closely related reference genomes (Mash/MinHash⁸³ distance ≤ 0.1 , corresponding to ANI $\geq 90\%$). At this similarity threshold, we assigned 640 out of the 1,000 MAGs from this study to neighbour groups containing as few as four to more than 100 members. Within each neighbour group and for each metabolic pathway, we tentatively assigned a binary phenotype value for a given MAG based on the neighbour-group genome with the closest matching gene annotation pattern (based on Hamming distance), even if some of the genes were absent in the query MAG. We limited comparisons to genes required for the function of each respective pathway.

Consensus phenotype predictions. We established a procedure to reconcile inconsistent phenotype predictions between the three strategies described above, based on observing discordant gene patterns and/or discordant predicted phenotypes within a given group of neighbour genomes. In the rare case of an irreconcilable disagreement between the prediction methods, assignment of a consensus phenotype defaulted to that produced by the machine-learning method. We assigned consensus confidence scores to each prediction on the basis of the degree of concordance between the three techniques and our confidence in the accuracy of each (Supplementary Discussion and Supplementary Table 7a). The complete phenotype prediction process was validated using the 2,856 reference genomes in the mcSEED database, their functionally annotated genes and the accompanying patterns of

presence/absence of functional metabolic pathways (curator-inferred binary phenotypes). The consensus phenotype predictions were combined into a binary phenotype matrix (BPM) containing 1,000 MAGs and 106 phenotypes (Supplementary Fig. 1, Supplementary Table 7a).

Gene annotation and phenotype prediction for *Bifidobacterium*-specific carbohydrate-utilization pathways. We adapted the annotation pipeline described above (Supplementary Fig. 1) to obtain functional annotations of genes comprising 25 additional carbohydrate-utilization pathways for a set of 34 *Bifidobacterium* MAGs, followed by inference of their respective binary phenotypes. As input data for this set of *Bifidobacterium*-specific phenotypes, we curated a set of 14 metabolic subsystems in 387 reference human-gut-derived *Bifidobacterium* genomes using the mcSEED framework. The reconstructed metabolic pathways and a corresponding BPM for reference *Bifidobacterium* genomes were used to predict carbohydrate-utilization phenotypes in the 34 *Bifidobacterium* MAGs. Finally, the automatically generated BPM was further manually curated to account for the variability of certain pathways in this taxonomically restricted set of predictions.

Applying enrichment analyses to predicted MAG phenotypes. Not all successfully annotated MAG genes were components of an intact functional pathway. To enable inferred phenotype-based analysis, we filtered gene annotations to those that were part of a complete functional pathway (with a respective binary phenotype value denoted as '1'). This filter resulted in a list of 208,246 genes used for microbiome and metatranscriptome phenotype enrichment analyses.

Annotation of CAZymes and PULs in *P. copri* MAGs and cultured *P. copri* strains

CAZymes were annotated according to the CAZy classification scheme⁸⁴. Amino acid sequences from MAGs and isolate genomes were analysed using a bioinformatics workflow that performs homology searches against the CAZy database⁸⁵ and specifically accommodates the modular structure of CAZymes (which often carry a variable number of ancillary modules in addition to their catalytic domain). Details of this workflow and its application are provided in a previous publication⁸⁶.

PULs were identified/predicted by combining information from marker genes (SusC/SusD pairs), operon structure and CAZyme annotation information, as previously described²⁴. The experimentally validated substrate specificities of CAZyme homologues contained in each PUL were used to infer the carbohydrate substrate(s) of each PUL.

We investigated the conservation of PULs within WLZ-associated *P. copri* MAGs and, subsequently, between these MAGs and all other *P. copri* MAGs and cultured *P. copri* isolate genomes from this study. As no automated method has been described to perform such a pan-genome PUL comparison, we proceeded manually through the following steps. First, we predicted the PUL repertoire of Bg0018 and Bg0019 using PULDB²⁵. Next, using Bg0019 as a reference, we selected PULs in Bg0018 and in other genomes for additional analysis if they displayed the same gene components in the same genomic order in both genomes. To do so, we conducted pairwise searches (BLASTp⁵¹) to identify homologous components (for example, SusC, SusD, transcriptional regulators, genes encoding CAZymes) of PULs in other *P. copri* genomes. The level of conservation for each PUL across the set of MAGs was categorized as (1) conserved (pairwise comparisons of ORFs satisfy the requirements that their protein products have >90% amino acid identity and that the ORFs comprising the PULs being compared are organized in an identical way within the respective genomes); (2) structurally distinct (a given PUL is present in the genomes being compared but one or more CAZymes or one or both SusC/SusD proteins are missing or fragmented in a way that is likely to impact their function, or where extra PUL ORFs are present); or (3) not conserved/absent

(PULs present in the respective genomes but with mutations that are likely to completely compromise function or where no PUL identified).

To relate the pattern of PUL conservation in *P. copri* MAGs to the WLZ response of study participants, we re-encoded each cell in the matrix shown in Fig. 4a as '1' for conserved PULs, '0.5' for structurally distinct PULs and '0' for not conserved/absent PULs. We imported this matrix into R, calculated a Euclidean distance between the PUL conservation pattern of Bg0019 and each additional MAG, then hierarchically clustered these patterns to generate a tree. Finally, we used Pearson correlation to relate the distance between the patterns of PUL conservation in Bg0019 and each additional *P. copri* MAG to the WLZ association (β_1 coefficient) of each MAG (Fig. 4b).

In vitro screening of glycan substrate specificity

We selected a variety of growth substrates representing putative glycan components of MDCF-2 plus glucose (Sigma-Aldrich, G8270) as a positive control and chondroitin sulfate (Thermo Fisher Scientific, J66156.06) as a negative control. Growth substrates included arabinan, arabinoxytan, β -glucan, galactan, galactomannan, rhamnogalacturonan, xyloglucan and xylan (all obtained from Neogen Megazyme; Supplementary Table 16a). A 2% (w/v) solution of each polysaccharide was prepared by mixing the polysaccharide with autoclaved, filter-purified water as recommended by the supplier (see Supplementary Table 16a for additional details of the preparation of each solution). Each solubilized substrate was allowed to equilibrate in the anaerobic growth chamber for around 5 days before use. Sterility was checked by (1) plating 10 μ l aliquots of each polysaccharide preparation onto BHI + 10% horse blood agar and (2) preparing 1:1 mixtures of preparation in *P. copri* defined medium (PCDM). This growth assay medium was selected because (1) it was fully defined, enabling supplementation with specific carbon sources and (2) it successfully supported the growth of *P. copri* strains in preliminary test cultures containing 5% glucose as the sole carbon source. PCDM was prepared according to the published recipe⁸⁷ with slight modifications (1 ml of a solution containing 1.9 mM haematin (H3281, Sigma-Aldrich) and 0.2 M L-histidine (Sigma-Aldrich, H6034) was added to each litre of the medium). Plates and broth were incubated for ≥ 3 days before checking for growth. The galactan and rhamnogalacturonan solutions displayed contamination. Thus, a fresh 2% (w/v) solution of each of these polysaccharides was prepared and autoclaved at 121 $^{\circ}$ C for 20 min at 15 psi before transferring them to the anaerobic chamber and confirming their sterility as described above. Autoclaved stocks were again checked for sterility before use.

We selected five *P. copri* isolates, representing a diversity of PUL conservation profiles, mcSEED BPMs and phylogenetic assignments for in vitro growth assays. Freezer stocks of each isolate were plated (~200 μ l) onto BHI + 10% horse blood and grown for 48 h at 37 $^{\circ}$ C. Isolated colonies were picked into 3 ml Wilkins-Chalgren medium and grown for 15 h at 37 $^{\circ}$ C. Each culture was then diluted 1:100 into fresh Wilkins-Chalgren medium and grown for an additional 6 h under the same anaerobic conditions at 37 $^{\circ}$ C to bring each culture into a similar phase of growth. The OD₆₀₀ was measured for each culture (Genesys 10S UV-Vis, Thermo Fisher Scientific) and the OD₆₀₀ was standardized to 0.02 by dilution into a final volume of 1 ml of PCDM with no added carbon source in a 96 \times 1.3 ml deep-well plate (Nunc, Thermo Fisher Scientific); this procedure enables us to have a uniform inoculum for all test isolates. A total of 9 ml of a 1:1 mixture of 2 \times PCDM containing 2% (w/v) glycan or control substrate was prepared in 50 ml polypropylene tubes (Corning) yielding 11 tubes of medium, each with an individual carbon source. These media plus the OD-standardized cultures were sealed (Alumaseal, Excel Scientific) and transferred to an anaerobic chamber containing a BioTek Precision XS liquid-handling robot. The robot was used to aliquot 180 μ l of each type of medium into corresponding columns of three 96-well flat-bottom tissue culture plates with a well capacity of 340 μ l (TPP, Sigma-Aldrich). A separate

Article

procedure on the Precision XS robot was used to mix and aliquot 20 µl of each OD₆₀₀-standardized culture into corresponding rows of each assay plate; one row was reserved as a no-inoculation control. Assay plates were then sealed with optically clear films (Axygen, UC-500) and placed into the input stack of a BioTek BioStack 4 microplate stacker configured to load a BioTek Eon microplate spectrophotometer. Before initiating the experiment, two heated catalyst boxes were used to warm the chamber to 37 °C. The microplate stacker and reader were used to perform 1 week of continuous monitoring, with OD₆₀₀ readings obtained every 15 min. Each assay plate was agitated for 5 s before each OD reading. At the conclusion of the experiment, data were exported in tabular form and analysed in R using custom scripts to determine maximal growth rate and OD₆₀₀ for each replicate of each culture in each glycan. Extracted curve parameters were normalized to growth rates determined in PCDM containing 5% glucose as the sole carbon source.

Biological materials

Faecal specimens collected from Bangladeshi children are the property of icddr,b. Material transfer agreements exist between icddr,b and Washington University in St Louis for the use of these samples. Requests for materials should be made to J.I.G and T.A.

Statistics and reproducibility

Statistical analyses were conducted using the approaches described in the Methods and the figure legends. Sample sizes and replicates are indicated along with each statistical test. All relevant statistical tests were two-tailed unless otherwise specified. All measurements were collected from distinct samples. Technical replicates were not collected and analysed unless otherwise noted.

Reporting summary

Further information on research design is available in the Nature Portfolio Reporting Summary linked to this article.

Data availability

Shotgun DNA sequencing and microbial RNA-seq datasets generated from faecal samples, plus annotated *P. copri* isolate genome sequences are available at the European Nucleotide Archive (PRJEB45356). These data were analysed to generate Figs. 1, 3 and 4, Extended Data Figs. 1, 2, 4, 5, 7, 8 and 10 and Supplementary Figs. 4 and 5. Anthropometry data from a previous publication⁴ were used in combination with data from the current study to generate Figs. 1b and 4b. The mcSEED database (<https://doi.org/10.5281/zenodo.10041395>) that was used to predict the presence or absence of metabolic pathways shown in Fig. 3, Extended Data Fig. 2 and Supplementary Figs. 1, 4 and 5 was described in a previous publication¹⁶. The CAZy^{84,85} and PULdb²⁵ databases were used to identify and analyse genes encoding carbohydrate-active enzymes and PULs in Figs. 4 and 5 and Extended Data Figs. 5 and 7–9. LC–MS datasets of monosaccharide, glycoside linkage and polysaccharide data are deposited in GlycoPOST (GPST000244) and were used to generate Figs. 2 and 5 and Extended Data Figs. 3, 6 and 7. All other relevant and/or supporting data are available in the Supplementary Information.

Code availability

Code detailing the steps in the MAG assembly workflow and analyses of microbial RNA-seq and glycan datasets are available at GitLab (https://gitlab.com/hibberdm/hibberd_webber_et_al_mdcb_poc_mags) and have been accessioned at Zenodo (<https://doi.org/10.5281/zenodo.8000098>). Code for annotation of bacterial genes and prediction of metabolic pathway presence/absence is available at GitHub (<https://github.com/rodionovdima/PhenotypePredictor>) and has been accessioned at Zenodo (<https://doi.org/10.5281/zenodo.10049439>).

- Baym, M. et al. Inexpensive multiplexed library preparation for megabase-sized genomes. *PLoS ONE* **10**, e0128036 (2015).
- Krueger, F., James, F., Ewels, P., Afyounian, E. & Schuster-Boeckler, B. TrimGalore, <https://doi.org/10.5281/zenodo.5127899> (2021).
- Langmead, B. & Salzberg, S. L. Fast gapped-read alignment with Bowtie 2. *Nat. Methods* **9**, 357–359 (2012).
- Li, D., Liu, C. M., Luo, R., Sadakane, K. & Lam, T. W. MEGAHIT: an ultra-fast single-node solution for large and complex metagenomics assembly via succinct de Bruijn graph. *Bioinformatics* **31**, 1674–1676 (2015).
- Bray, N. L., Pimentel, H., Melsted, P. & Pachter, L. Near-optimal probabilistic RNA-seq quantification. *Nat. Biotechnol.* **34**, 525–527 (2016).
- Wu, Y. W., Simmons, B. A. & Singer, S. W. MaxBin 2.0: an automated binning algorithm to recover genomes from multiple metagenomic datasets. *Bioinformatics* **32**, 605–607 (2016).
- Kang, D. D. et al. MetaBAT 2: an adaptive binning algorithm for robust and efficient genome reconstruction from metagenome assemblies. *PeerJ* **7**, e7359 (2019).
- Sieber, C. M. K. et al. Recovery of genomes from metagenomes via a dereplication, aggregation and scoring strategy. *Nat. Microbiol.* **3**, 836–843 (2018).
- Bertrand, D. et al. Hybrid metagenomic assembly enables high-resolution analysis of resistance determinants and mobile elements in human microbiomes. *Nat. Biotechnol.* **37**, 937–944 (2019).
- Walker, B. J. et al. Pilon: an integrated tool for comprehensive microbial variant detection and genome assembly improvement. *PLoS ONE* **9**, e112963 (2014).
- Parks, D. H., Imelfort, M., Skennerton, C. T., Hugenholtz, P. & Tyson, G. W. CheckM: assessing the quality of microbial genomes recovered from isolates, single cells, and metagenomes. *Genome Res.* **25**, 1043–1055 (2015).
- Nayfach, S., Shi, Z. J., Seshadri, R., Pollard, K. S. & Kyrpides, N. C. New insights from uncultivated genomes of the global human gut microbiome. *Nature* **568**, 505–510 (2019).
- Olm, M. R., Brown, C. T., Brooks, B. & Banfield, J. F. dRep: a tool for fast and accurate genomic comparisons that enables improved genome recovery from metagenomes through de-replication. *ISME J.* **11**, 2864–2868 (2017).
- Gurevich, A., Saveliev, V., Vyahhi, N. & Tesler, G. QUAST: quality assessment tool for genome assemblies. *Bioinformatics* **29**, 1072–1075 (2013).
- Seemann, T. Prokka: rapid prokaryotic genome annotation. *Bioinformatics* **30**, 2068–2069 (2014).
- Schaeffer, L., Pimentel, H., Bray, N., Melsted, P. & Pachter, L. Pseudoalignment for metagenomic read assignment. *Bioinformatics* **33**, 2082–2088 (2017).
- Wood, D. E., Lu, J. & Langmead, B. Improved metagenomic analysis with Kraken 2. *Genome Biol.* **20**, 257 (2019).
- Lu, J., Breitwieser, F. P., Thielen, P. & Salzberg, S. Bracken: estimating species abundance in metagenomics data. *PeerJ Comput. Sci.* **3**, e104 (2017).
- Asnicar, F. et al. Precise phylogenetic analysis of microbial isolates and genomes from metagenomes using PhyloPhlAn 3.0. *Nat. Commun.* **11**, 2500 (2020).
- Asnicar, F., Weingart, G., Tickle, T. L., Huttenhower, C. & Segata, N. Compact graphical representation of phylogenetic data and metadata with GraPhlAn. *PeerJ* **3**, e1029 (2015).
- Page, A. J. et al. Roary: rapid large-scale prokaryote pan genome analysis. *Bioinformatics* **31**, 3691–3693 (2015).
- Altschul, S. F., Gish, W., Miller, W., Myers, W. W. & Lipman, D. J. Basic local alignment search tool. *J. Mol. Biol.* **215**, 403–410 (1990).
- Katoh, K. & Standley, D. M. MAFFT multiple sequence alignment software version 7: improvements in performance and usability. *Mol. Biol. Evol.* **30**, 772–780 (2013).
- Snipen, L. & Hovde Liland, K. microseq: basic biological sequence handling. R package version 2.1.5, CRAN.R-project.org/package=microseq (2021).
- Nguyen, L. T., Schmidt, H. A., von Haeseler, A. & Minh, B. Q. IQ-TREE: a fast and effective stochastic algorithm for estimating maximum-likelihood phylogenies. *Mol. Biol. Evol.* **32**, 268–274 (2015).
- Love, M. I., Huber, W. & Anders, S. Moderated estimation of fold change and dispersion for RNA-seq data with DESeq2. *Genome Biol.* **15**, 550 (2014).
- Bates, D., Mächler, M., Bolker, B. & Walker, S. Fitting linear mixed-effects models using lme4. *J. Stat. Softw.* **67**, 1–48 (2015).
- Kuznetsova, A., Brockhoff, P. B. & Christensen, R. H. B. lmerTest package: tests in linear mixed effects models. *J. Stat. Softw.* **82**, 1–26 (2017).
- Hoffman, G. E. & Roussos, P. Dream: powerful differential expression analysis for repeated measures designs. *Bioinformatics* **37**, 192–201 (2020).
- Andrews, S. FastQC: a quality control tool for high throughput sequence data (2010); www.bioinformatics.babraham.ac.uk/projects/fastqc/.
- McCarthy, D. J., Chen, Y. & Smyth, G. K. Differential expression analysis of multifactor RNA-seq experiments with respect to biological variation. *Nucleic Acids Res.* **40**, 4288–4297 (2012).
- Korotkevich, G. et al. Fast gene set enrichment analysis. Preprint at [bioRxiv](https://doi.org/10.1101/060012) <https://doi.org/10.1101/060012> (2021).
- Kassambara, A. & Mundt, F. factoextra: extract and visualize the results of multivariate data analyses. R package version 1.0.7, CRAN.R-project.org/package=factoextra (2020).
- Oksanen, J. et al. vegan: community ecology package. R package version 2.5-7, CRAN.R-project.org/package=vegan (2020).
- Xu, G., Amicucci, M. J., Cheng, Z., Galermo, A. G. & Lebrilla, C. B. Revisiting monosaccharide analysis—quantitation of a comprehensive set of monosaccharides using dynamic multiple reaction monitoring. *Analyst* **143**, 200–207 (2018).
- Amicucci, M. J. et al. A rapid-throughput adaptable method for determining the monosaccharide composition of polysaccharides. *Intern. J. Mass Spectrom.* **438**, 22–28 (2019).
- Galermo, A. G. et al. Liquid chromatography–tandem mass spectrometry approach for determining glycosidic linkages. *Anal. Chem.* **90**, 13073–13080 (2018).
- Galermo, A. G., Nandita, E., Castillo, J. J., Amicucci, M. J. & Lebrilla, C. B. Development of an extensive linkage library for characterization of carbohydrates. *Anal. Chem.* **91**, 13022–13031 (2019).

68. Nandita, E. et al. Polysaccharide identification through oligosaccharide fingerprinting. *Carbohydr. Polym.* **257**, 117570 (2021).
69. Han, N. D. et al. Microbial liberation of *N*-methylserotonin from orange fiber in gnotobiotic mice and humans. *Cell* **185**, 2495–2509 (2022).
70. Kolmogorov, M. et al. Assembly of long, error-prone reads using repeat graphs. *Nat. Biotechnol.* **37**, 540–546 (2019).
71. Price, M. N. et al. FastTree 2—approximately maximum-likelihood trees for large alignments. *PLoS ONE* **5**, e9490 (2010).
72. Paradis, E. & Schliep, K. ape 5.0: an environment for modern phylogenetics and evolutionary analyses in R. *Bioinformatics* **35**, 526–528 (2018).
73. Yu, G. Using ggtree to visualize data on tree-like structures. *Curr. Protoc. Bioinform.* **69**, e96 (2020).
74. Davis, J. J. et al. The PATRIC Bioinformatics Resource Center: expanding data and analysis capabilities. *Nucleic Acids Res.* **48**, D606–D612 (2020).
75. Ye, Y., Osterman, A., Overbeek, R. & Godzik, A. Automatic detection of subsystem/pathway variants in genome analysis. *Bioinformatics* **21**, i478–i486 (2005).
76. Steinegger, M. & Söding, J. MMseqs2 enables sensitive protein sequence searching for the analysis of massive data sets. *Nat. Biotechnol.* **35**, 1026–1028 (2017).
77. Buchfink, B., Reuter, K. & Drost, H. G. Sensitive protein alignments at tree-of-life scale using DIAMOND. *Nat. Methods* **18**, 366–368 (2021).
78. Hyatt, D. et al. Prodigal: prokaryotic gene recognition and translation initiation site identification. *BMC Bioinform.* **11**, 119 (2010).
79. Schubert, E. et al. DBSCAN revisited, revisited: why and how you should (still) use DBSCAN. *ACM Trans. Database Syst.* **42**, 1–21 (2017).
80. Pedregosa, F. et al. Scikit-learn: machine learning in python. *J. Mach. Learn. Res.* **12**, 2825–2830 (2011).
81. Therneau, T., Atkinson, B. & Ripley, B., Rpart: recursive partitioning, github.com/bethatkinson/rpart/ (2013).
82. Kuhn, M. Building predictive models in R using the caret package. *J. Stat. Softw.* **28**, 1–26 (2008).
83. Ondov, B. D. et al. Mash: fast genome and metagenome distance estimation using MinHash. *Genome Biol.* **17**, 132 (2016).
84. Drula, E. et al. The carbohydrate-active enzyme database: functions and literature. *Nucleic Acids Res.* **50**, D571–D577 (2021).
85. Lombard, V., Ramulu, H. G., Drula, E., Coutinho, P. M. & Henrissat, B. The carbohydrate-active enzymes database (CAZy) in 2013. *Nucleic Acids Res.* **42**, D490–D495 (2014).
86. Delannoy-Bruno, O. et al. Evaluating microbiome-directed fibre snacks in gnotobiotic mice and humans. *Nature* **595**, 91–95 (2021).
87. Li, J. et al. A versatile genetic toolbox for *Prevotella copri* enables studying polysaccharide utilization systems. *EMBO J.* **40**, e108287 (2021).

Acknowledgements We thank M. Meier, J. Serugo, S. Deng, K. Ahsan, J. Hoisington-Lopez and M. Crosby for technical assistance; members of the Genome Technology Access Center at

Washington University School of Medicine for Illumina NovaSeq-based generation of faecal DNA shotgun sequencing and microbial RNA-seq datasets; and E. Martin and B. Koebbe for high-performance computing support. This work was supported by the Bill & Melinda Gates Foundation, the National Institutes of Health (DK30292) and the Washington University-Centene Personalized Medicine Initiative. J.I.G. is the recipient of an Agilent Thought Leader Award.

Author contributions M.C.H. and D.M.W. generated short-read and long-read shotgun sequencing datasets of faecal DNAs and, together with H.M.L., assembled MAGs. D.A.R., A.L.O., M.D.K., S.A.L. and A.A.A. performed metabolic pathway reconstruction and annotation of MAGs, while S.H., V.L., N.T. and B.H. annotated PULs and CAZymes in MAGs. M.C.H. identified WLZ-correlated MAGs and conducted analyses of the enrichment of their encoded functions. M.C.H. and R.Y.C. conducted analyses of MAG abundance responses to treatment. D.M.W. generated and together with M.C.H., C.Z., D.A.R., A.L.O. and A.A.A. analysed microbial RNA-seq datasets. J.J.C., C.B.L., G.C., N.P.B. and Y.C. performed LC–MS analyses of food and faecal glycans. J.L.-G. isolated *P. copri* strains with assistance from D.M.W. and M.C.H. M.C.H., D.M.W. and S.H. designed the in vitro growth experiments, which were performed by M.C.H., D.M.W. and S.H. with assistance from J.L.-G. Y.W., H.-W.C. and E.M.L. integrated the results of MAG-based analysis described in this paper with findings from ‘reverse translation’ experiments involving gnotobiotic mice and cultured *P. copri* strains. I.M., S.D. and M.M., under the supervision of T.A., conducted the clinical study of MDCF-2 and RUSF and supplied all of the biospecimens used for the analyses conducted in this report. M.J.B. oversaw databases of clinical metadata and the biospecimen archive. T.A. and J.I.G. oversaw this research. M.C.H., D.M.W. and J.I.G. wrote the paper with input from all of the other authors.

Competing interests A.L.O. and D.A.R. are co-founders of Phenobiome, a company pursuing development of computational tools for predictive phenotype profiling of microbial communities. C.B.L. is a co-founder of Inifant Health, interVenn Bio and BCD Bioscience—companies involved in the characterization of glycans and developing carbohydrate applications for human health. A joint patent application between Washington University in St Louis and icddr,b has been filed, entitled “Synbiotic combination of selected strains of *P. copri* and dietary glycans to treat malnutrition”, with J.I.G., M.C.H., D.M.W., H.-W.C., Y.W., M.J.B. and T.A. listed as co-inventors (PCT/US2023/018738). The authors are committed to the principle of Global Access; patented technologies will be made available and accessible at an affordable price to those in need throughout the world.

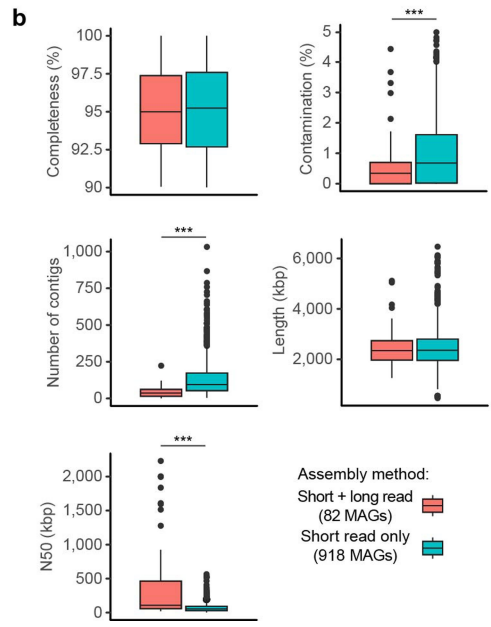
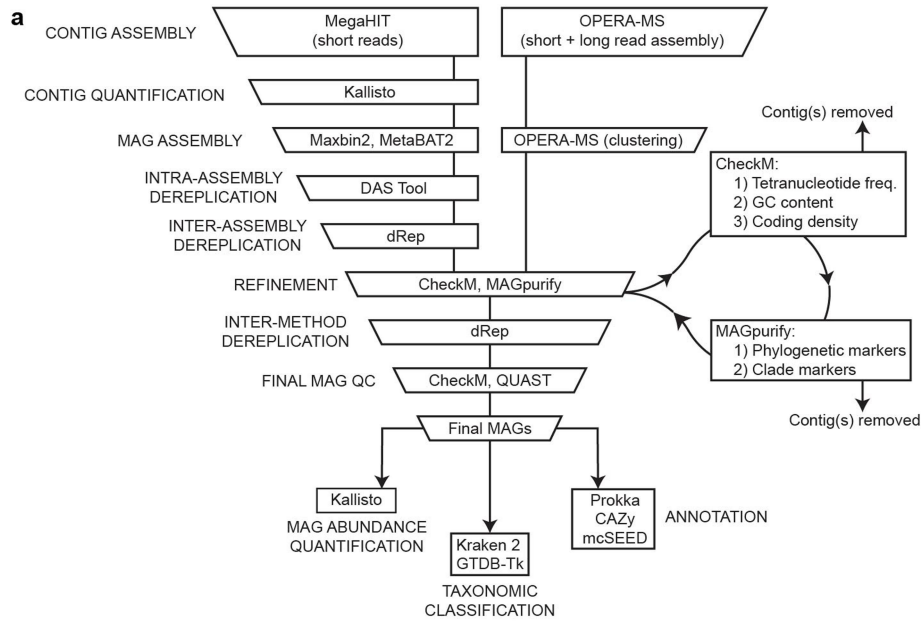
Additional information

Supplementary information The online version contains supplementary material available at <https://doi.org/10.1038/s41586-023-06838-3>.

Correspondence and requests for materials should be addressed to Jeffrey I. Gordon.

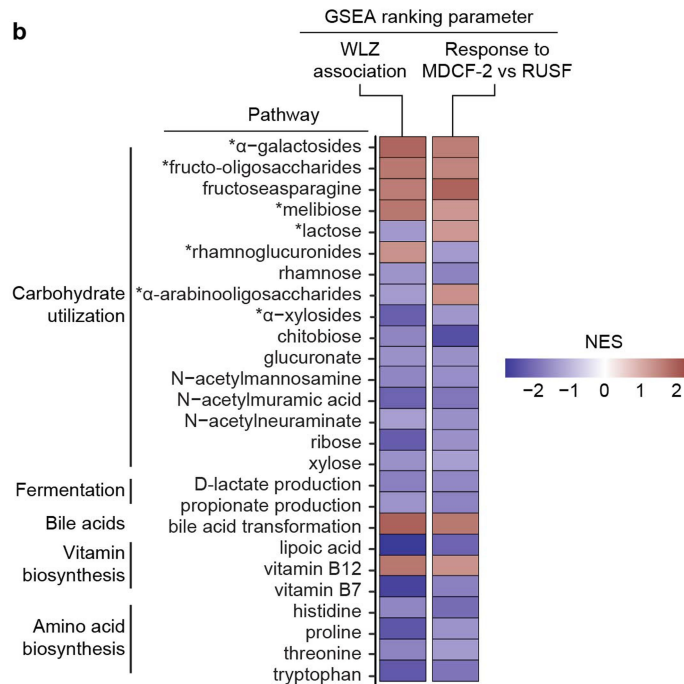
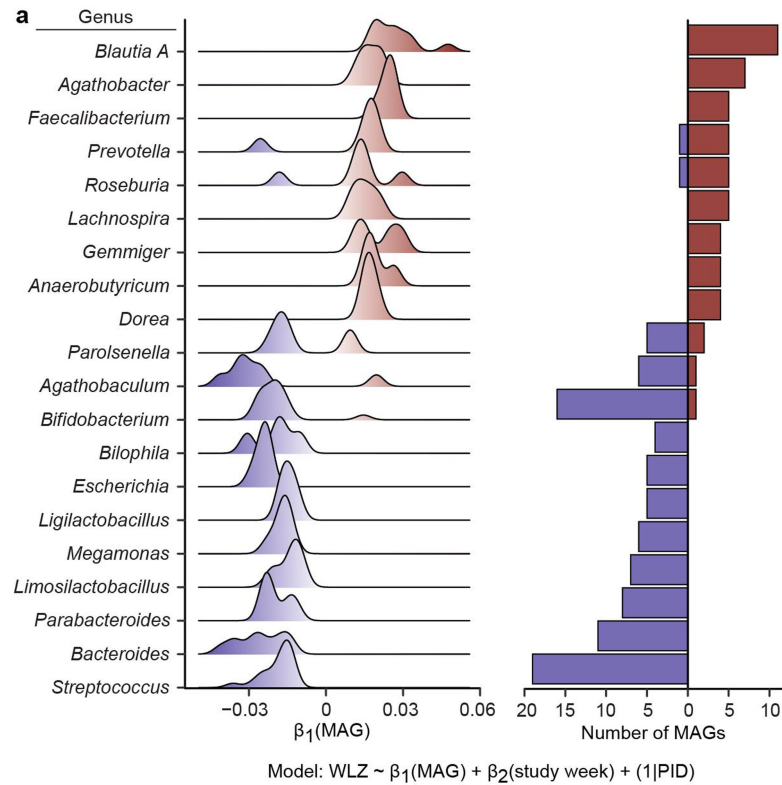
Peer review information *Nature* thanks the anonymous reviewer(s) for their contribution to the peer review of this work.

Reprints and permissions information is available at <http://www.nature.com/reprints>.



Extended Data Fig. 1 | Bioinformatic workflow for MAG assembly, refinement, and quantitation. (a) Pipeline for MAG assembly from short-read only or short-read plus long-read shotgun sequencing data. Steps are indicated alongside the boxes, while the bioinformatic tools employed to accomplish each step are described within each box. (b) Comparison of MAG assembly summary statistics derived from CheckM (completeness, contamination) or Quast (number, length and N50 of contigs) for n = 82 high-quality MAGs obtained

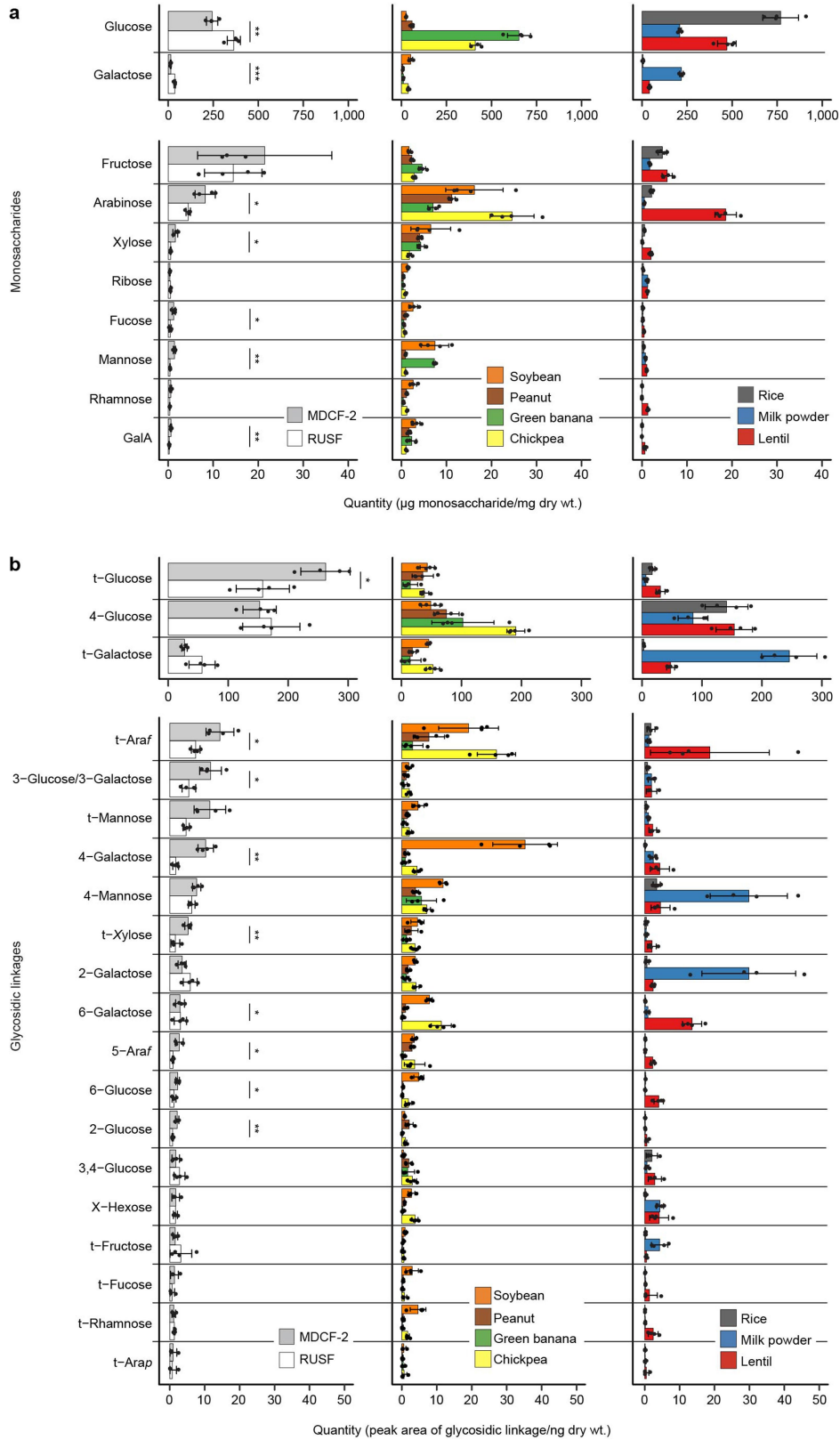
from short- plus long-read hybrid assemblies versus n = 918 high-quality MAGs from short-read only assembly methods. MAGs were assembled from shotgun sequencing data obtained from n = 942 biologically independent faecal samples as described in *Methods*. Boxplots show the median, first and third quartiles; whiskers extend to the largest value no further than 1.5 × the interquartile range. ***, $P < 0.001$ (Wilcoxon test, two-sided).



Extended Data Fig. 2 | Taxonomy and functional characteristics of

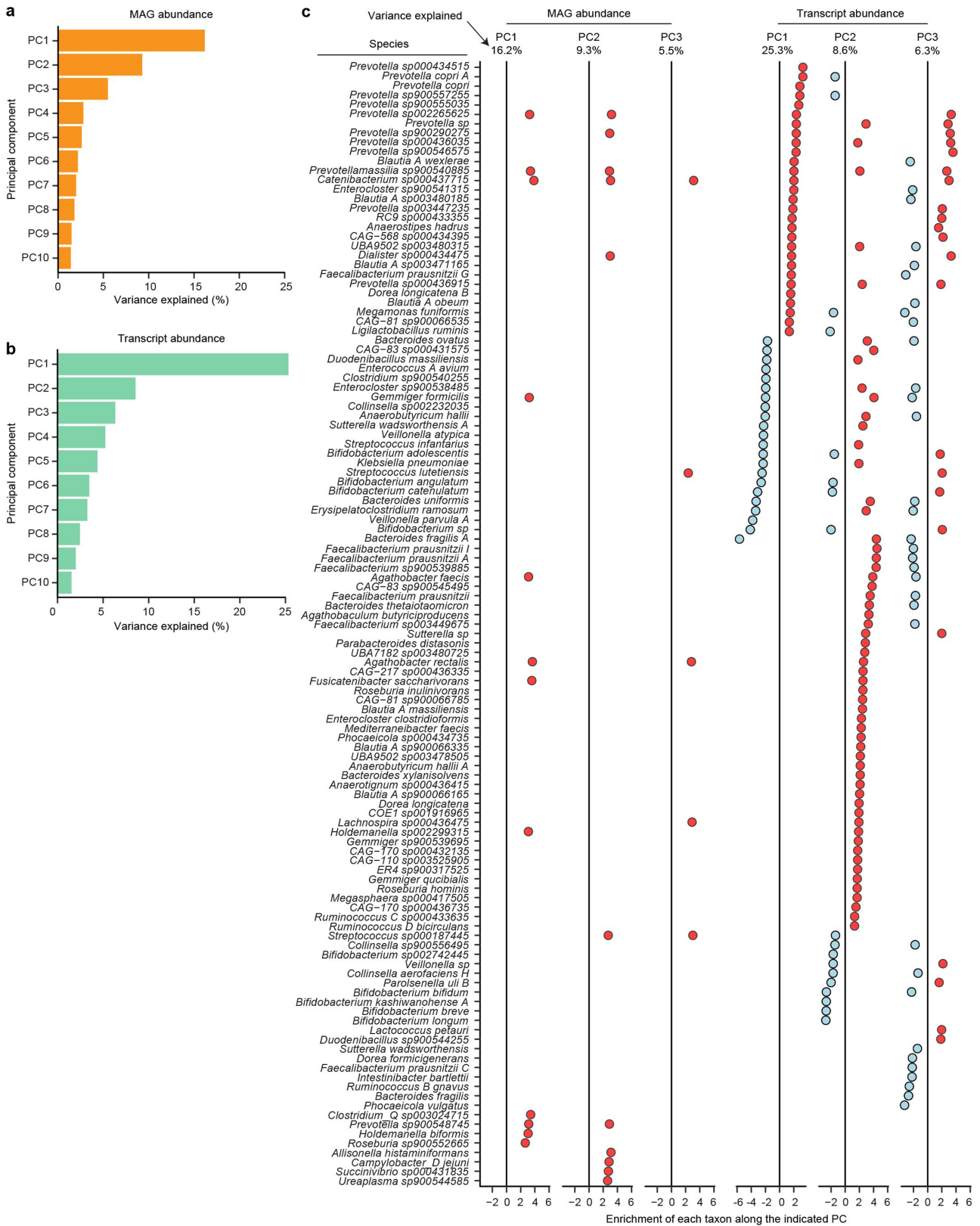
WLZ-associated MAGs. (a) Left subpanel, density plot showing WLZ-associated MAGs tabulated based on their genus-level classification. β_1 refers to the coefficient in the linear mixed effects model presented at the bottom of the figure. Genera containing >3 significantly WLZ-associated MAGs are shown. Right subpanel, number of statistically significant WLZ-associated MAGs assigned to each genus depicted in the left subpanel. (b) Enrichment of metabolic pathways in WLZ- and treatment-associated MAGs. MAGs were

ranked by their WLZ association (negative to positive) or treatment association (RUSF-associated to MDCF-2-associated) and GSEA was employed to determine overrepresentation of pathways in MAGs at the extremes of each ranked list. The results (Normalized Enrichment Score, NES) only include pathways that display a statistically significant enrichment ($q < 0.05$, GSEA) in both the WLZ-associated MAG and treatment-associated MAG analyses. For carbohydrate utilization pathways, disaccharides and oligosaccharides are indicated with an asterisk.



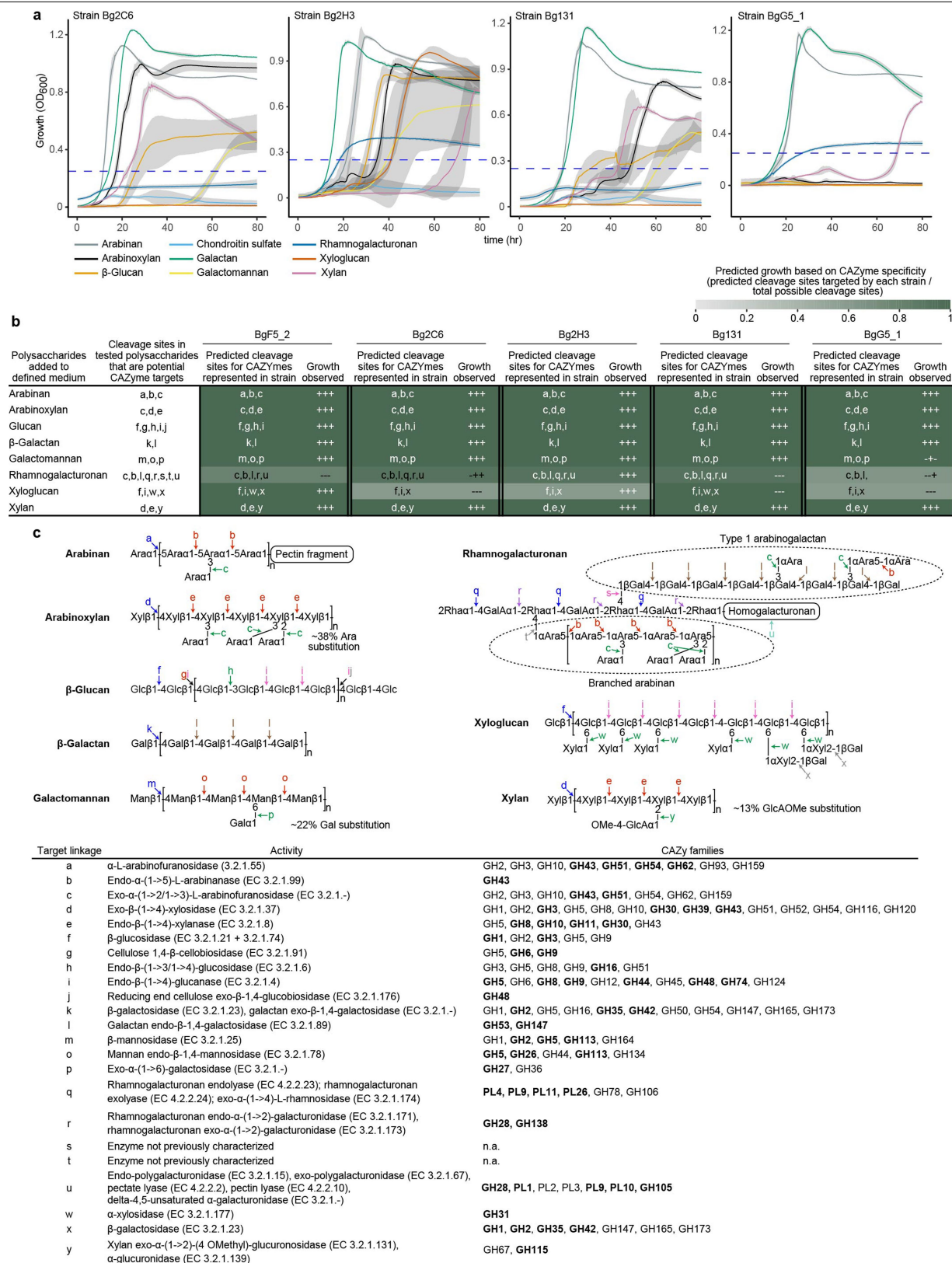
Extended Data Fig. 3 | LC-MS analysis of glycans present in MDCF-2, RUSF and their component ingredients. (a, b) Analysis of monosaccharides (panel a) and glycosidic linkages (panel b) liberated by hydrolysis of glycans present in

MDCF-2 and RUSF, and in the food ingredients used to formulate them. Mean \pm SD are plotted for $n = 4$ independent samples. *, $P < 0.05$, **, $P < 0.01$ (t-test, two-sided). Points depict individual samples.



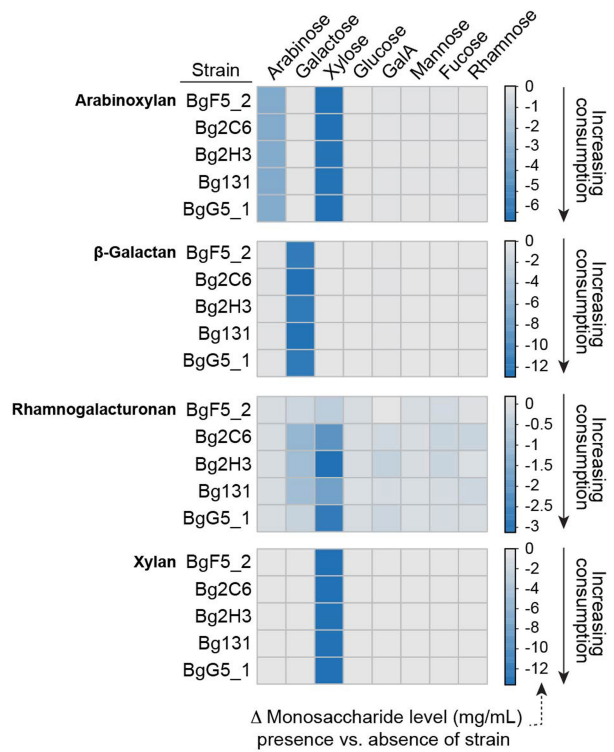
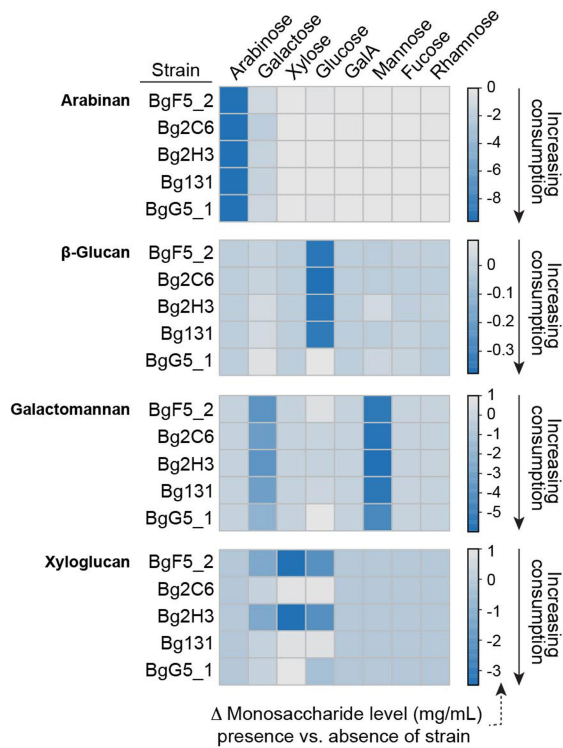
Extended Data Fig. 4 | Principal components analysis of transcript and MAG abundances in faecal specimens. (a, b) Percent variance explained by the top 10 principal components of a PCA analysis including abundance of MAGs (panel a) at the 0, 2, 4, 8, 12, and 16 week time points in Fig. 1a, or transcripts

(panel b) at 0, 4, and 12 weeks. (c) Significantly enriched taxa ($q < 0.05$, GSEA) along the first three principal components (PC1-PC3) of the faecal microbiome or meta-transcriptome PCA.



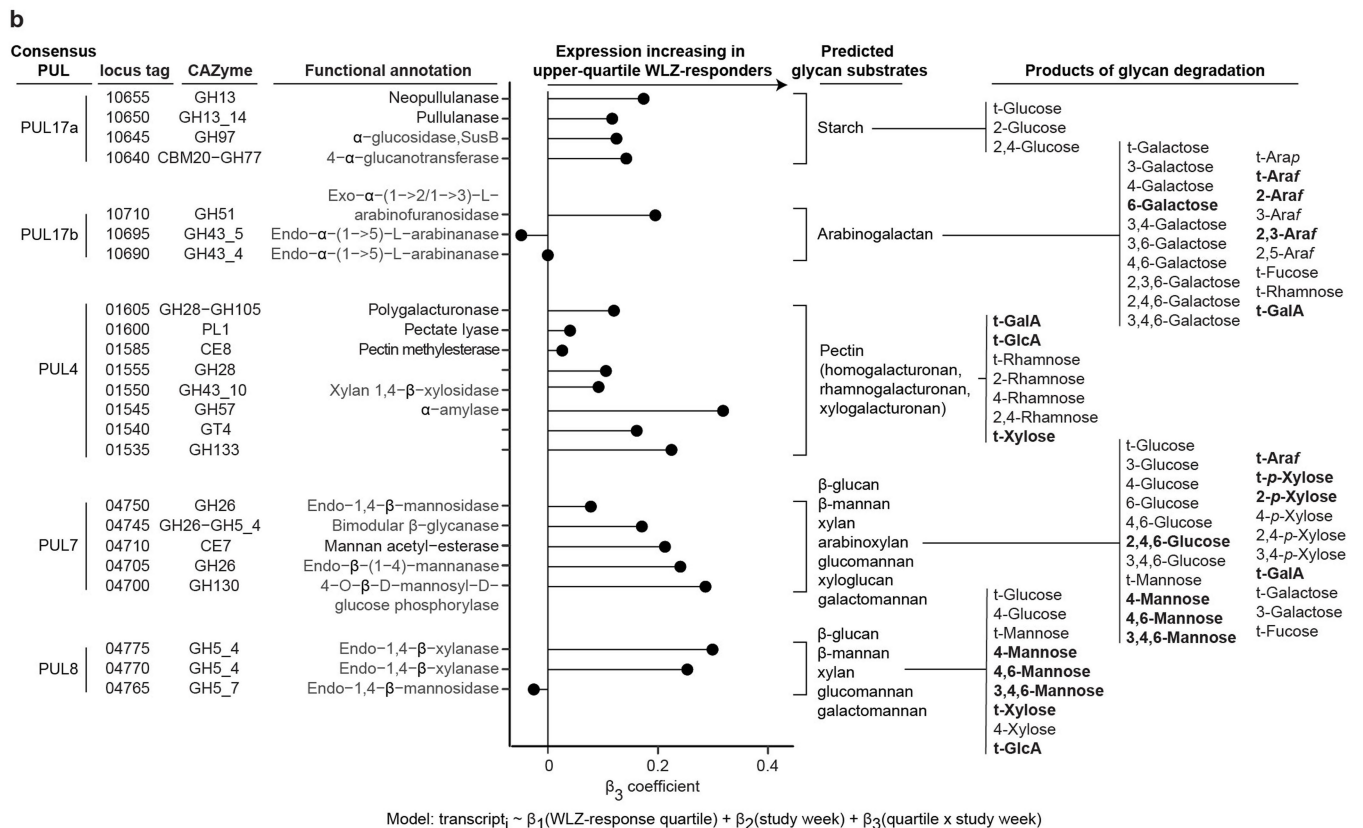
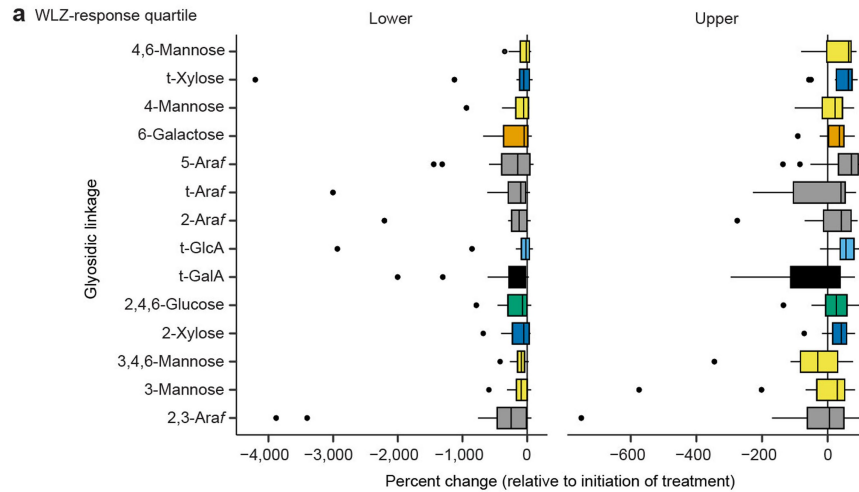
Extended Data Fig. 5 | Growth of Bangladeshi *P. copri* strains in defined medium supplemented with purified polysaccharides. (a) Growth curves in defined medium containing individual purified polysaccharides similar to those that are abundant in or unique to MDCF-2 compared to RUSF. Curves describe mean values \pm sd for OD₆₀₀ measurements (n = 3 replicates/growth condition). (b) Growth of *P. copri* strains versus a PUL-based prediction of their growth phenotypes. Growth is expressed as '+' or '-' for each of the triplicate cultures according to whether a threshold OD₆₀₀ > 0.25 was attained. The colour key

expresses 'prediction' as the fraction of possible cleavage sites in each polysaccharide that are known or predicted to be targeted by the PUL-associated CAZymes of a given strain. (c) CAZymes present in the PULs of each strain and their predicted activities against glycosidic linkages in each purified polysaccharide. Linkages in a polysaccharide that are predicted to be targeted by PUL-associated CAZymes are labelled 'a,b,...y' in both panels b and c. All CAZyme family assignments for a given enzymatic activity are shown; the family that displays this activity most commonly is noted in bold font.



Extended Data Fig. 6 | LC-MS analysis of monosaccharide consumption during growth of cultured Bangladeshi *P. copri* strains in defined medium supplemented with purified polysaccharides. Heatmaps representing bacterial consumption of monosaccharides present in the different polysaccharides. UHPLC-QqQ-MS-based monosaccharide analysis was performed using defined medium harvested from monocultures of the *P. copri*

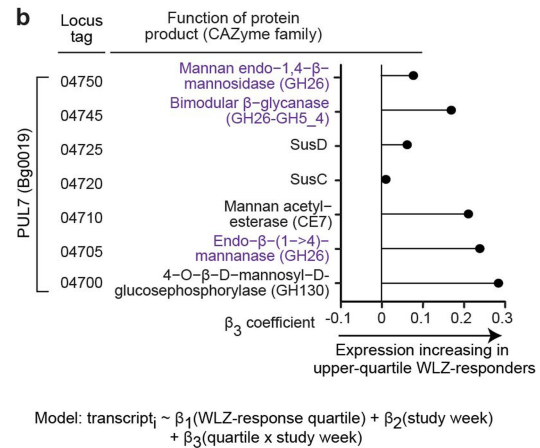
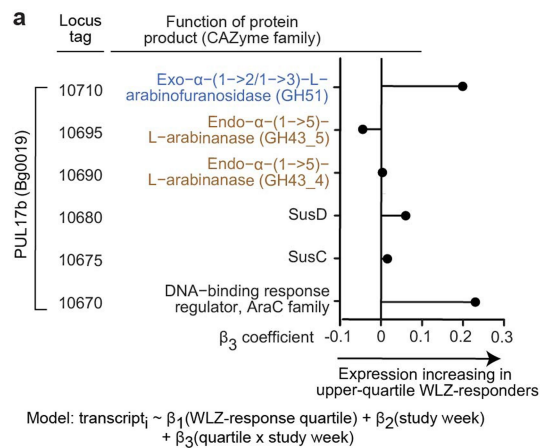
strains. Control incubations did not contain added bacteria. Cells in each matrix show the mean difference (at the end of the 189 hour-long incubation) between the concentration of each monosaccharide in three technical replicates of each strain/polysaccharide combination compared to the corresponding uninoculated control.



Model: transcript_i ~ β₁(WLZ-response quartile) + β₂(study week) + β₃(quartile x study week)

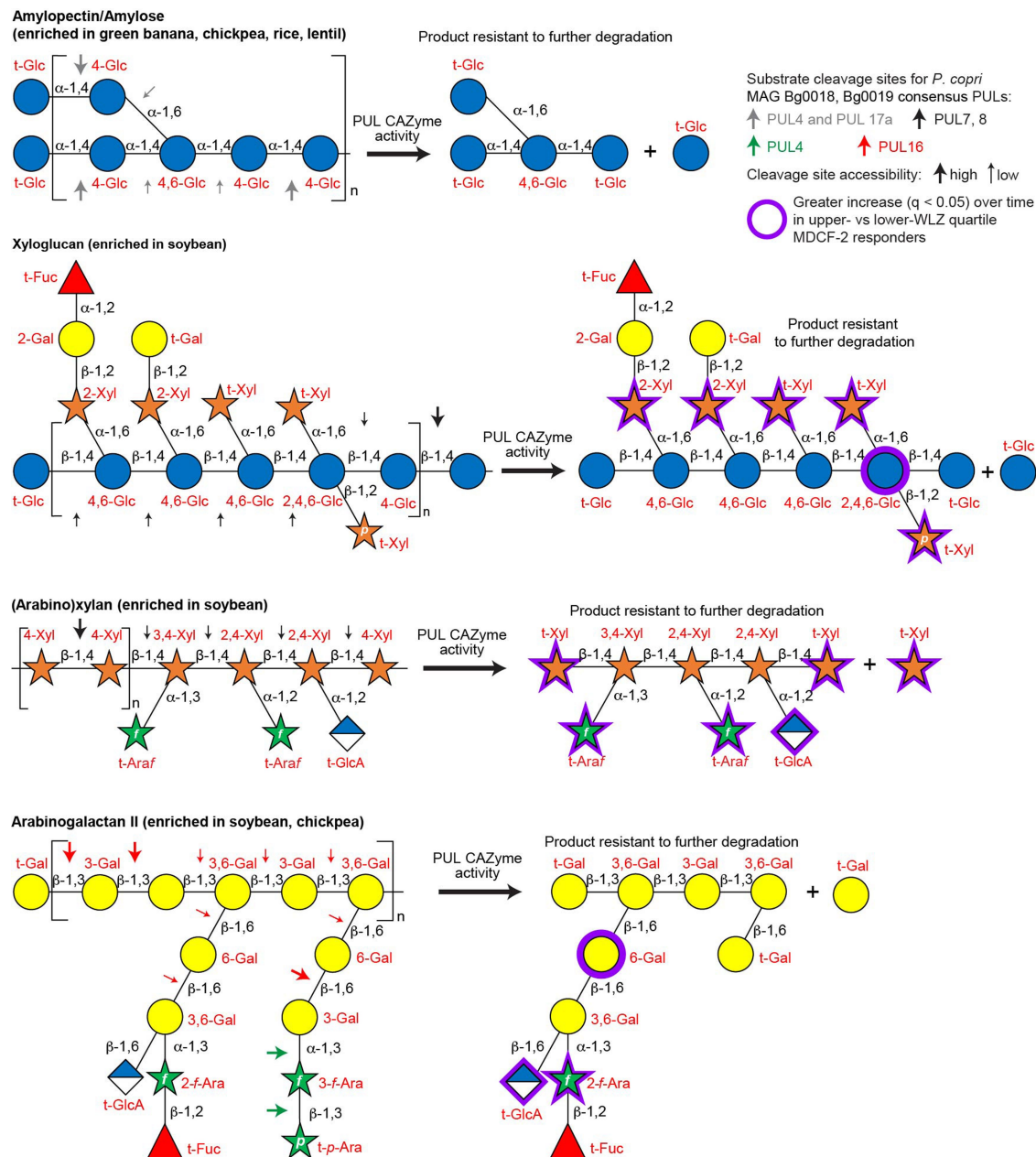
Extended Data Fig. 7 | Changes in levels of faecal glycosidic linkages and expression of *P. copri* CAZyme genes after MDCF-2 treatment. (a) Boxplot of changes in the levels of faecal glycosidic linkages relative to initiation of treatment among upper and lower WLZ quartile responders. Levels of these 14 linkages increased to a significantly greater extent over time in the upper vs lower WLZ response quartiles (Model: linkage abundance - WLZ-response quartile × study week + (1|PID)). Boxplots indicate the median, first and third quartiles; whiskers extend to the largest value no further than 1.5 × the interquartile range for 90 biologically independent faecal samples obtained

from n = 15 participants assigned to the upper quartile and n = 15 participants assigned to the lower quartile of WLZ-responses (n = 3 samples/participant). (b) The β₃ coefficient for the interaction of WLZ-response quartile and study week is shown for CAZymes in consensus PULs in Bg0018 and Bg0019. Predicted PUL substrates and potential glycosidic linkages in each of these substrates are shown on the right. Glycosidic linkages whose abundances were significantly different in faecal samples from the upper versus lower WLZ quartile responders are highlighted in bold font (see Fig. 5a).



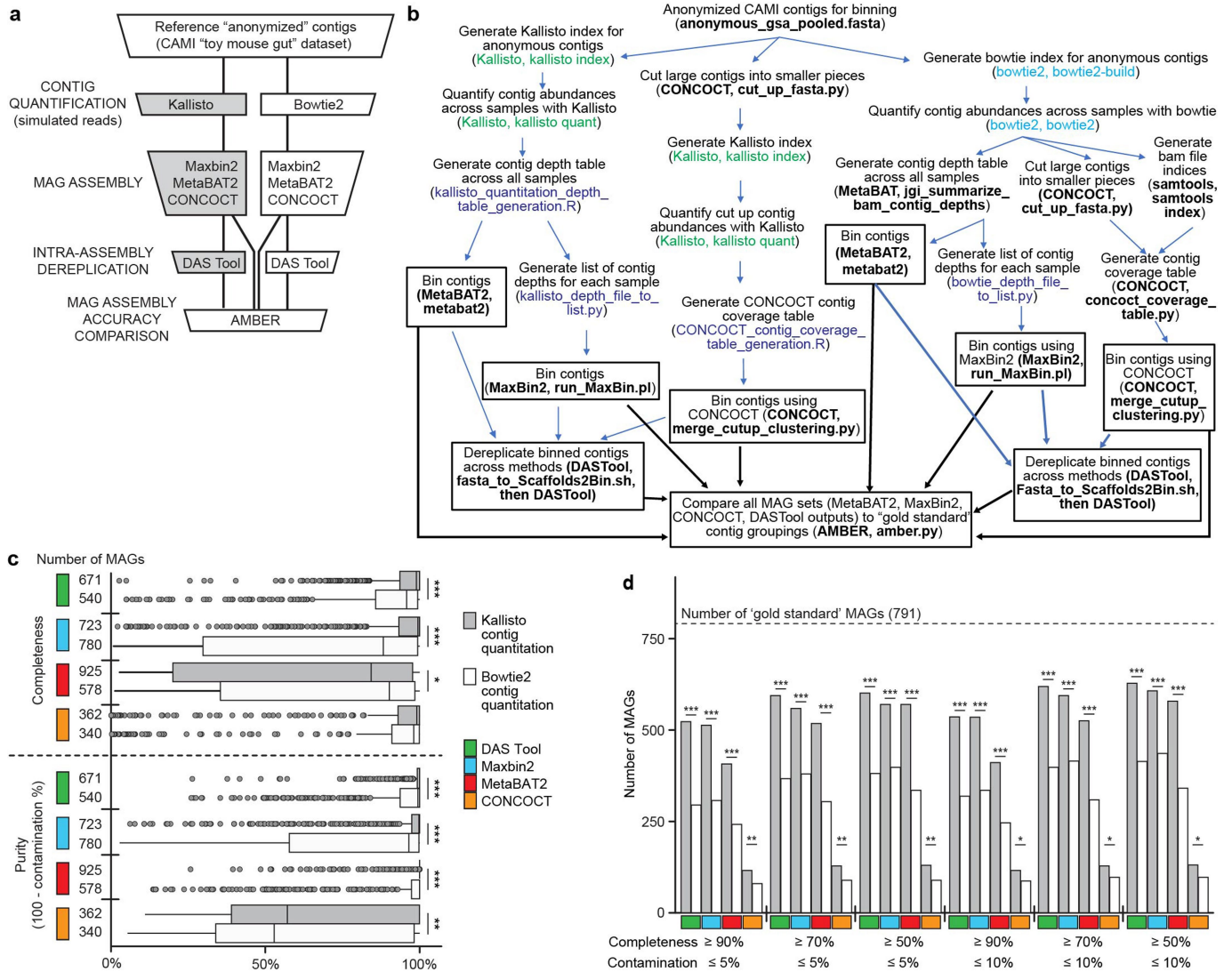
Extended Data Fig. 8 | Treatment-responsive glycosidic linkages and corresponding polysaccharide sources and structures, cleavage sites, and predicted products of CAZyme activity. (a,b) Predicted activities and expression of *P. copri* PUL CAZymes. Panel a depicts CAZymes assigned to PUL17b, including (i) the GH51 family CAZyme (blue) expected to cleave α -1,2- and α -1,3-linked arabinofuranose (Araf) side chains and (ii) GH43_4 and GH43_5 subfamily members (brown) predicted to cleave α -1,5-Araf-linked backbone of

branched arabinan, yielding products containing *t*-Araf, 2-Araf, 2,3 Araf and 5-Araf linkages. Panel b depicts CAZymes assigned to PUL7, including GH26 and GH5_4 CAZymes (magenta) predicted to cleave β -1,4 linked mannose residues of galactomannan, yielding products containing 4,6-mannose which is the most significantly differentially abundant linkage in the upper quartile WLZ responders (see Fig. 5a). The CAZyme colouring scheme matches that used in Fig. 5b, c.



Extended Data Fig. 9 | Polysaccharide structures, cleavage sites, and predicted products of CAZyme activity. Glycosidic linkages highlighted with arrows are those predicted as sites of cleavage by CAZymes expressed by the set of PULs, described in Fig. 4a, that are present in *P. copri* MAG Bg0019 and/or Bg0018. Consensus PUL numbers are listed except in the case of Bg0019 PUL3,

which is not represented in Bg0018 (see Supplementary Table 15). The size of the arrows (large versus small) denotes the relative likelihood (high versus low, respectively) of cleavage of glycosidic linkages by *P. copri* CAZymes when considering steric hindrance at branch points.



Extended Data Fig. 10 | Validation of the MAG assembly pipeline.

(a) Bioinformatic workflow for comparing the fidelity of MAG assembly from alignment-based (bowtie2) versus pseudoalignment-based (kallisto) contig quantitation. **(b)** A detailed description of the workflow is described in panel a. Each box includes a summary of the computational task plus the name of the program and, where relevant, the command used to complete the task (in parentheses). Colour of the text in parentheses: brown, default code from kallisto; purple, default code from bowtie2; blue, custom script written to achieve tasks described; black, default code used for programs to assemble MAGs and dereplicate contigs. Boxes with a black outline and the thick black arrows emanating from them indicate that binned contigs were used as input to AMBER for MAG assembly comparisons across methods. **(c)** Boxplot describing summary statistics (completeness and purity) for MAG assembly approaches.

(d) Number of MAGs, obtained from each assembly and quantitation strategy, that are distributed across two quality metrics (completeness, contamination). The number of 'gold standard' MAGs (theoretical maximum) in the simulated metagenomic dataset is indicated by a horizontal dashed line. *, $P < 0.05$; **, $P < 0.01$; ***, $P < 0.001$ (two-tailed, unpaired Wilcoxon test for panel c; two-tailed Fisher's exact test for panel d).

Reporting Summary

Nature Portfolio wishes to improve the reproducibility of the work that we publish. This form provides structure for consistency and transparency in reporting. For further information on Nature Portfolio policies, see our [Editorial Policies](#) and the [Editorial Policy Checklist](#).

Statistics

For all statistical analyses, confirm that the following items are present in the figure legend, table legend, main text, or Methods section.

n/a Confirmed

- The exact sample size (n) for each experimental group/condition, given as a discrete number and unit of measurement
- A statement on whether measurements were taken from distinct samples or whether the same sample was measured repeatedly
- The statistical test(s) used AND whether they are one- or two-sided
Only common tests should be described solely by name; describe more complex techniques in the Methods section.
- A description of all covariates tested
- A description of any assumptions or corrections, such as tests of normality and adjustment for multiple comparisons
- A full description of the statistical parameters including central tendency (e.g. means) or other basic estimates (e.g. regression coefficient) AND variation (e.g. standard deviation) or associated estimates of uncertainty (e.g. confidence intervals)
- For null hypothesis testing, the test statistic (e.g. F , t , r) with confidence intervals, effect sizes, degrees of freedom and P value noted
Give P values as exact values whenever suitable.
- For Bayesian analysis, information on the choice of priors and Markov chain Monte Carlo settings
- For hierarchical and complex designs, identification of the appropriate level for tests and full reporting of outcomes
- Estimates of effect sizes (e.g. Cohen's d , Pearson's r), indicating how they were calculated

Our web collection on [statistics for biologists](#) contains articles on many of the points above.

Software and code

Policy information about [availability of computer code](#)

Data collection No specialized software or code was used for data collection

Data analysis The following software packages were used to analyze the data in this study: Trim Galore3 (v0.6.4), bowtie2 (v2.3.4.1), MegaHit (v1.1.4), MaxBin2 (v2.2.5), MetaBAT2 (v2.12.1), DAS Tool (v1.1.2), OPERA-MS (v0.9.0), CheckM (v1.1.3), MAGpurify (v2.1.2), dRep (v2.6.2), prokka (v1.14.6), GTDB-Tk (v1.3.0), Kraken2 (v2.0.8), Bracken (v2.5), PhyloPhlan (v3.0.60), Graphlan (v1.1.4), Roary (v3.12.0), MAFFT (v7.3.13), microseq R package (v2.1.4), IQ-TREE (v1.6.12), kallisto (v0.43.0), DESeq2 (v1.34.0), lme4 (v1.1-27.1), lmerTest (v3.1-3), dream variancePartition R package (v1.24.0), FastQC (v0.11.7), edgeR37 (v3.32.1), factoextra (v1.0.7), vegan R package (v2.5-7), ggtree (v3.2.1), ape (v5.6-2), MMSeqs (v1-c7a89), DIAMOND (v2.0.0), prodigal (v2.6.3), Scikit-learn (v0.22.1), Rpart (v4.1.15), Caret (v6.0.86). Code detailing the steps in the MAG assembly workflow and analyses of microbial RNA-Seq and glycan datasets are available from GitLab (https://gitlab.com/hibberdm/hibberd_webber_et_al_mdcb_poc_mags) and have been accessioned at Zenodo (DOI:10.5281/zenodo.8000098). Code for annotation of bacterial genes and prediction of metabolic phenotypes is available from GitHub (<https://github.com/rodionovdima/PhenotypePredictor>) and has been accessioned at Zenodo (DOI: 10.5281/zenodo.10049439).

For manuscripts utilizing custom algorithms or software that are central to the research but not yet described in published literature, software must be made available to editors and reviewers. We strongly encourage code deposition in a community repository (e.g. GitHub). See the Nature Portfolio [guidelines for submitting code & software](#) for further information.

Data

Policy information about [availability of data](#)

All manuscripts must include a [data availability statement](#). This statement should provide the following information, where applicable:

- Accession codes, unique identifiers, or web links for publicly available datasets
- A description of any restrictions on data availability
- For clinical datasets or third party data, please ensure that the statement adheres to our [policy](#)

Shotgun DNA sequencing and microbial RNA-Seq datasets generated from fecal samples, plus annotated *P. copri* isolate genome sequences are available in the European Nucleotide Archive (accession PRJEB45356). Anthropometry data is available from a prior publication (ref. 4; DOI: 10.1056/NEJMoa2023294). The mcSEED database (<https://zenodo.org/records/10041396>) was used to predict the presence or absence of metabolic pathways. The Genome Taxonomy Database (GTDB) was used as a reference for taxonomic classification of MAGs. The CAZy and PULdb databases were used to identify and analyze carbohydrate-active genes and PULs. LC-MS datasets of monosaccharide, glycoside linkage, and polysaccharide data are deposited in GlycoPOST (accession GPST000244). All other relevant and/or supporting data is available in the Supplementary Information.

Field-specific reporting

Please select the one below that is the best fit for your research. If you are not sure, read the appropriate sections before making your selection.

- Life sciences Behavioural & social sciences Ecological, evolutionary & environmental sciences

For a reference copy of the document with all sections, see nature.com/documents/nr-reporting-summary-flat.pdf

Life sciences study design

All studies must disclose on these points even when the disclosure is negative.

Sample size	Target enrollment for the clinical trial was set at 124 participants (n=62 per arm). This sample size was calculated to achieve 80% power at a 5% significance level for detecting a treatment effect. The anticipated effect size was derived from changes in Weight-for-Length Z-score (WLZ) observed in a pilot randomized, double-blind controlled feeding study (ref. 3, DOI: 10.1126/science.aau4732). A total of 123 participants were randomized in the clinical trial (n=61 MDCF-2 diet, 62 RUSF diet), and 59 children in each group completed the 3-month intervention and 1-month follow-up and were included in our analyses. Additional details on the clinical trial design and sample size calculations are available elsewhere (ref. 4 [DOI: 10.1056/NEJMoa2023294], DOI 10.1186/s12889-020-8330-8).
Data exclusions	Participants who did not complete the trial were excluded as described previously (ref. 4 [DOI: 10.1056/NEJMoa2023294]). No additional data were excluded from the analyses described in the current study.
Replication	To enhance reproducibility, the MAG assembly pipeline was validated using synthetic sequence data from CAMI II as indicated in Extended Data Fig. 10. This validation measured the fidelity of MAG assembly, the accuracy of kallisto-based MAG quantification, and the effects of filtering as described in the supplementary information. We employed a consensus-based approach for assigning annotations as a means of enhancing the reliability of these metabolic pathway annotations. We utilized both short- and long-read MAG assembly methods and compared these assembly methods as illustrated in Extended Data Fig. 10. We compared results from two methods of taxonomic assignment and utilized a consensus approach to assign MAG taxonomy in a reproducible manner. The capacity of <i>P. copri</i> strains to utilize specific carbohydrate substrates was validated using a series of in vitro growth experiments as illustrated in Extended Data Fig. 5.
Randomization	Eligible participants, whose parents/guardians provided written informed consent, were randomly assigned to treatment groups. Participant randomization was performed by an independent researcher who has had no involvement in the trial (please see an additional description of randomization: DOI 10.1186/s12889-020-8330-8).
Blinding	Participants were blinded to their treatment group. Study staff were blinded to the extent that was possible as described in DOI 10.1186/s12889-020-8330-8. Investigators were not blinded to group allocation when analyzing the data presented in this paper.

Reporting for specific materials, systems and methods

We require information from authors about some types of materials, experimental systems and methods used in many studies. Here, indicate whether each material, system or method listed is relevant to your study. If you are not sure if a list item applies to your research, read the appropriate section before selecting a response.

Materials & experimental systems

n/a	Involvement
<input checked="" type="checkbox"/>	<input type="checkbox"/> Antibodies
<input checked="" type="checkbox"/>	<input type="checkbox"/> Eukaryotic cell lines
<input checked="" type="checkbox"/>	<input type="checkbox"/> Palaeontology and archaeology
<input checked="" type="checkbox"/>	<input type="checkbox"/> Animals and other organisms
<input type="checkbox"/>	<input checked="" type="checkbox"/> Human research participants
<input type="checkbox"/>	<input checked="" type="checkbox"/> Clinical data
<input checked="" type="checkbox"/>	<input type="checkbox"/> Dual use research of concern

Methods

n/a	Involvement
<input checked="" type="checkbox"/>	<input type="checkbox"/> ChIP-seq
<input checked="" type="checkbox"/>	<input type="checkbox"/> Flow cytometry
<input checked="" type="checkbox"/>	<input type="checkbox"/> MRI-based neuroimaging

Human research participants

Policy information about [studies involving human research participants](#)

Population characteristics	Please refer to Chen, Mostafa, Hibberd et al., "A Microbiota-Directed Food Intervention for Undernourished Children", N Engl J Med 2021 (DOI: 10.1056/NEJMoa2023294) for population characteristics.
Recruitment	Please refer to Chen, Mostafa, Hibberd et al., "A Microbiota-Directed Food Intervention for Undernourished Children", N Engl J Med 2021 (DOI: 10.1056/NEJMoa2023294) for recruitment information.
Ethics oversight	The study protocol was approved by the Ethical Review Committee at the International Center for Diarrheal Disease Research, Bangladesh (icddr,b)

Note that full information on the approval of the study protocol must also be provided in the manuscript.

Clinical data

Policy information about [clinical studies](#)

All manuscripts should comply with the ICMJE [guidelines for publication of clinical research](#) and a completed [CONSORT checklist](#) must be included with all submissions.

Clinical trial registration	ClinicalTrials.gov identifier: NCT04015999
Study protocol	The human biospecimens analyzed in this manuscript are from a previously reported clinical study. The protocol for this study is detailed in ref. 4 (N Engl J Med 2021 (DOI: 10.1056/NEJMoa2023294).
Data collection	The human biospecimens analyzed in this manuscript are from a previously reported clinical study. The data collection methods for this study are detailed in ref. 4 (N Engl J Med 2021 (DOI: 10.1056/NEJMoa2023294).
Outcomes	The human biospecimens analyzed in this manuscript are from a previously reported clinical study. The primary and secondary outcome measures for this study are detailed in ref. 4 (N Engl J Med 2021 (DOI: 10.1056/NEJMoa2023294).